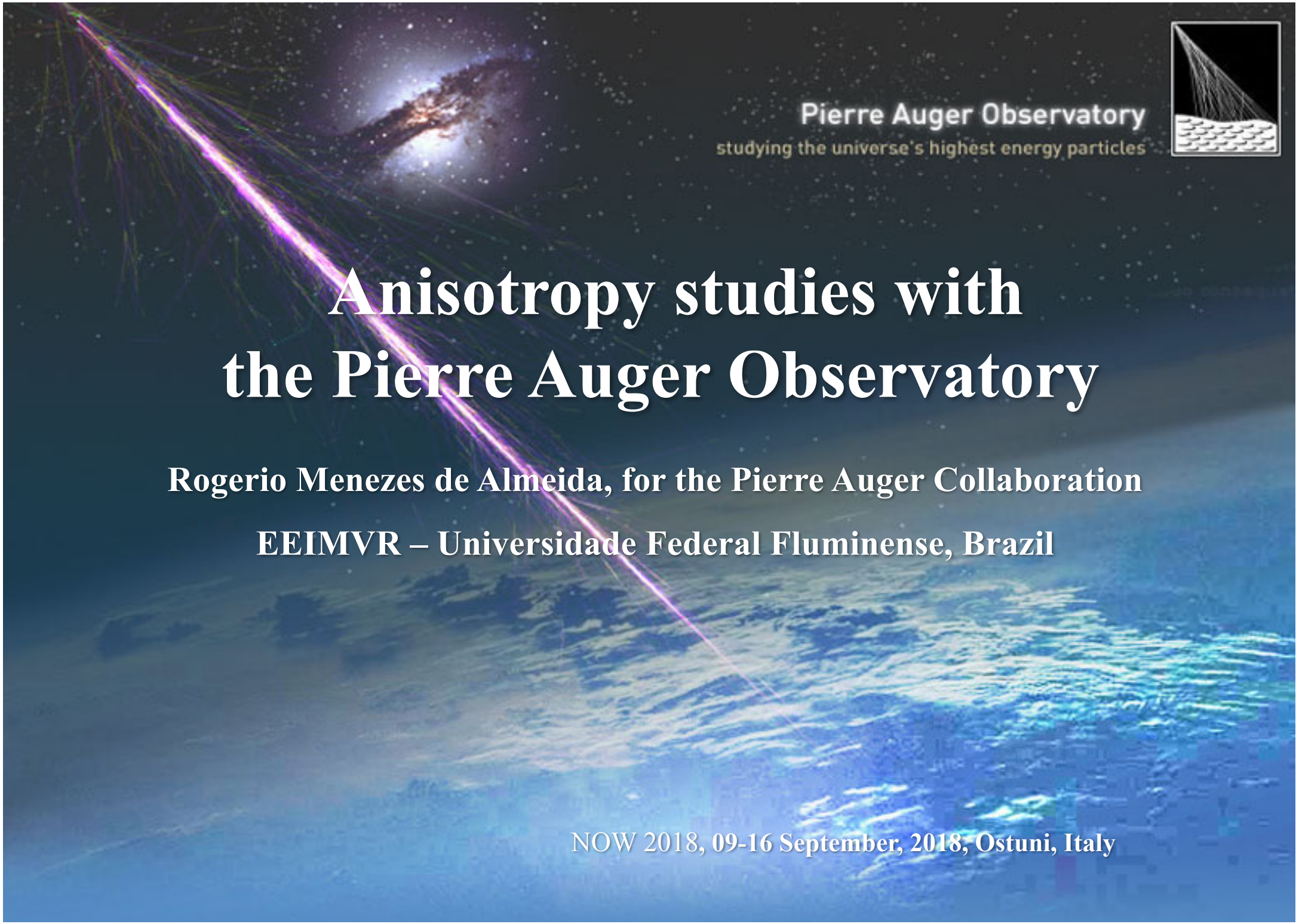

Anisotropy studies with the Pierre Auger Observatory

Rogerio Menezes de Almeida, for the Pierre Auger Collaboration

EEIMVR – Universidade Federal Fluminense, Brazil

NOW 2018, **09-16 September, 2018, Ostuni, Italy**

Outline

- Brief introduction to the Pierre Auger Observatory
- Auger energy spectrum
- Mass composition
- Arrival Directions
  - Indication for intermediate-scale anisotropy

    ApJ.Lett. 853:L29 (2018)

  - Observation of Large-scale anisotropy

    Science 357 (2017) 1266
    submitted to ApJ, arXiv:1808.03579

The Pierre Auger Observatory

~ 500 members, 17 countries

Main Detectors

Surface detector

- array of 1660 Cherenkov stations on a 1.5 km hexagonal grid ~ 3000 km^2
- duty cycle ~ 100%

Fluorescence detector

- 4 + 1 buildings overlooking the array (24 + 3) telescopes
- duty cycle ~ 13%

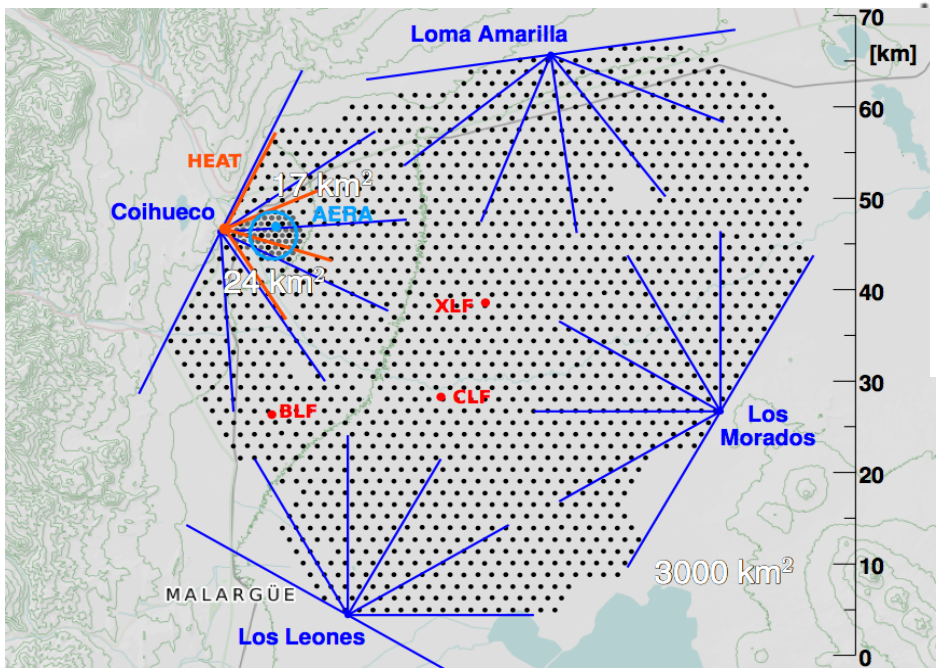

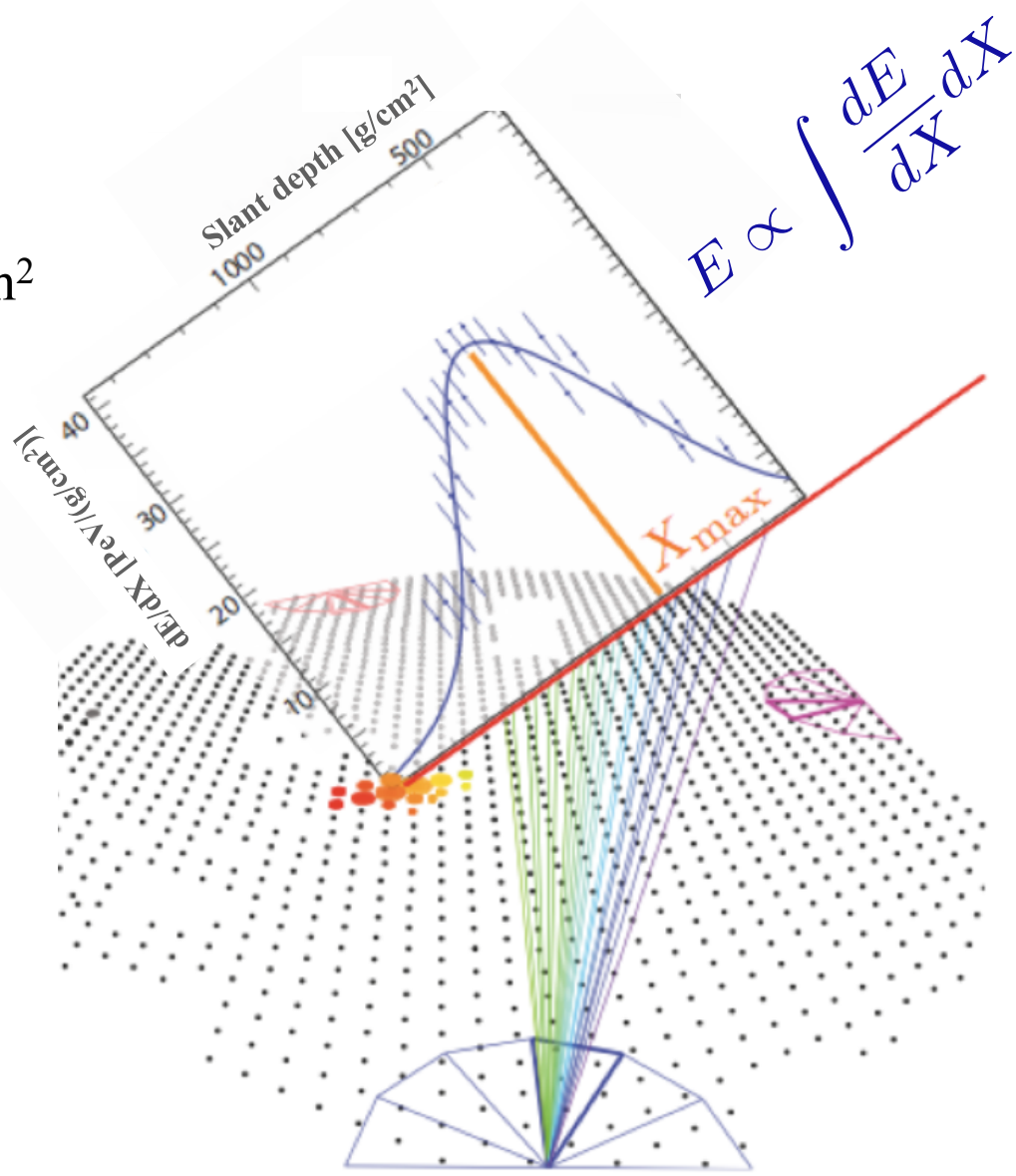

Malargue, Argentina

Auger Energy Spectrum

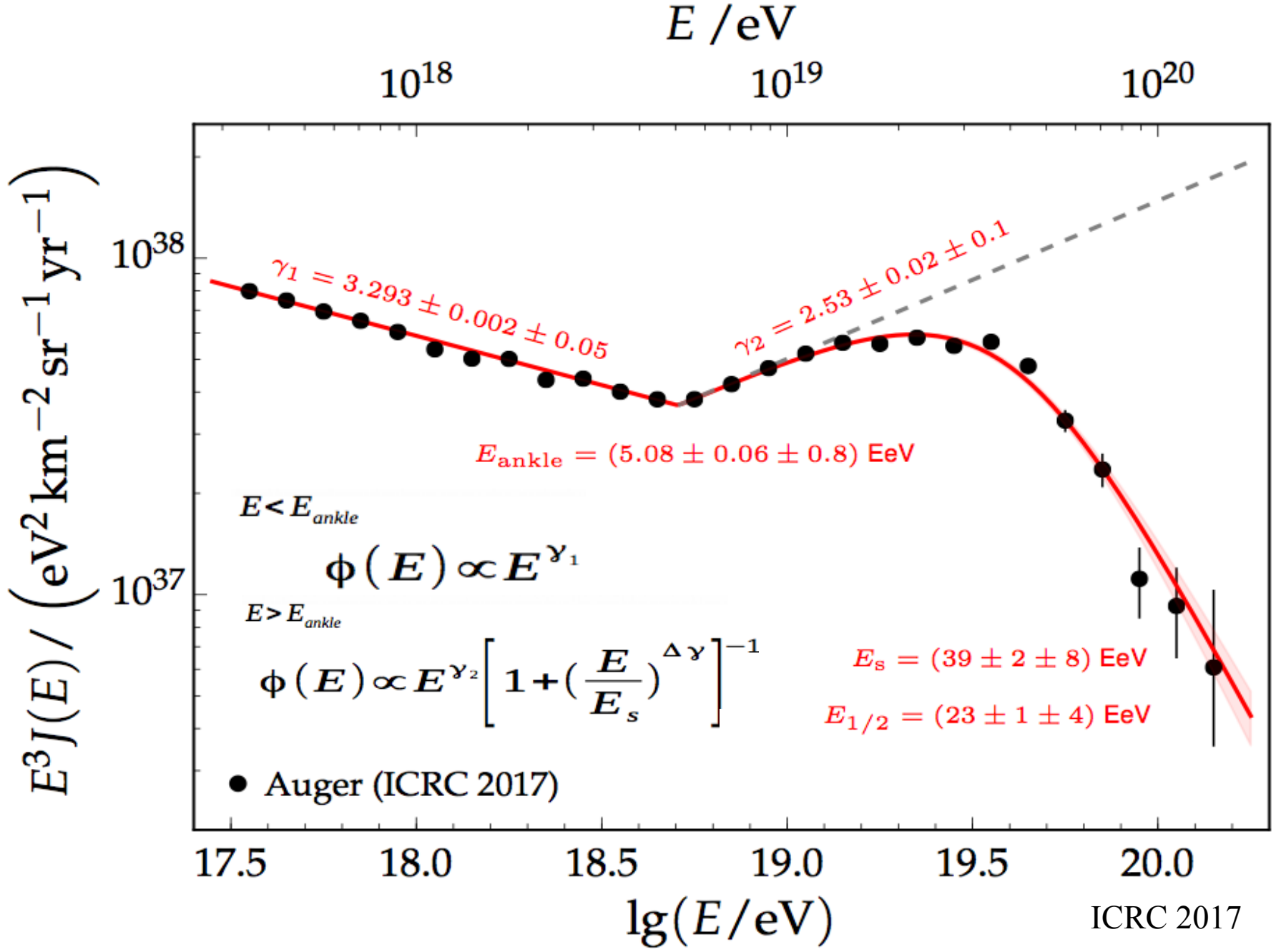

ICRC 2017

Average X_{max} and X_{max} fluctuations

ICRC 2017

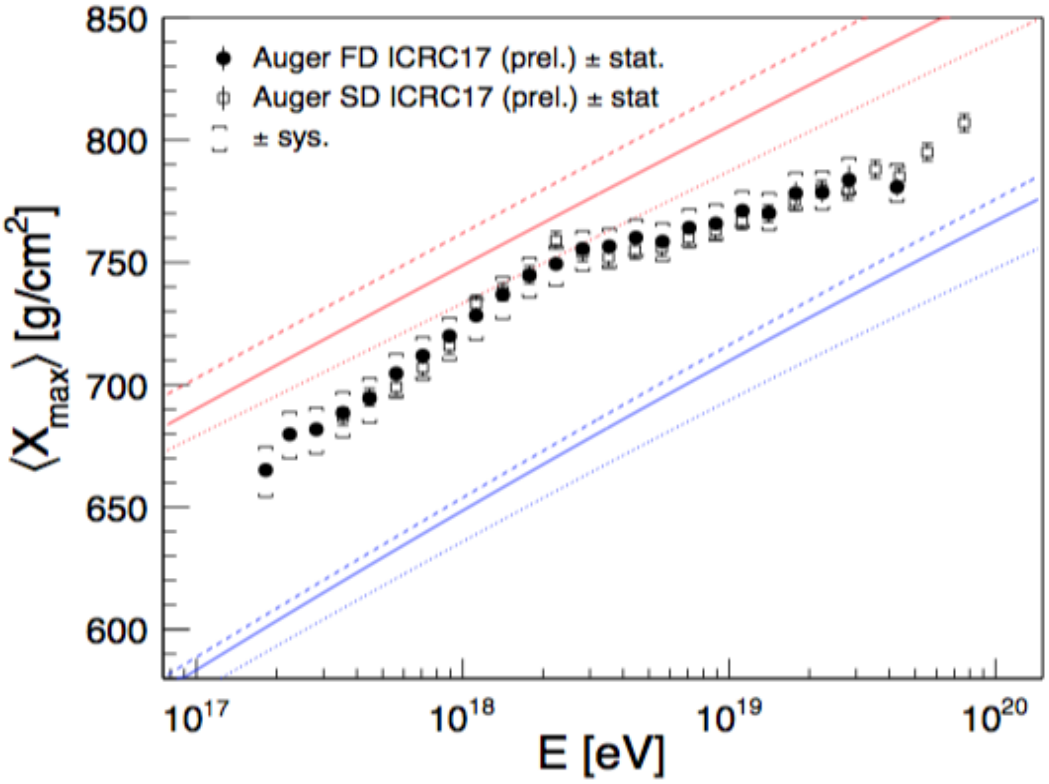

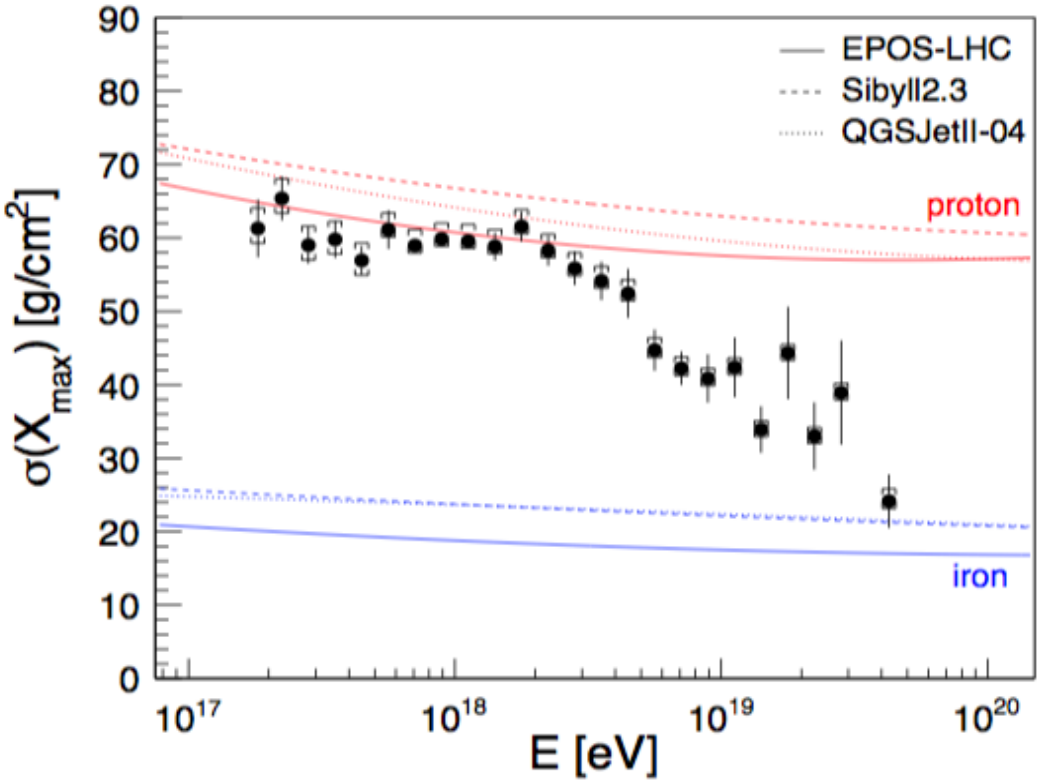

Mixed composition at the highest energies

Arrival Directions

- Indication for intermediate-scale anisotropy

  ApJ.Lett. 853:L29 (2018)853:L29

- Observation of Large-scale anisotropy

  Science 357 (2017) 1266
  submitted to ApJ, arXiv:1808.03579

Arrival Directions

- Indication for intermediate-scale anisotropy

  ApJ.Lett. 853:L29 (2018)853:L29

- Observation of Large-scale anisotropy

  Science 357 (2017) 1266
  submitted to ApJ, arXiv:1808.03579

Search for Intermediate-scale Anisotropies

Study motivated by Fermi-LAT observations of high-energy gamma rays

- SBG: 23 nearby starburst galaxies, $\Phi > 0.3$ Jy, w : radio at 1.4 GHz
- γAGN: 17 2FHL blazars and radio galaxies, $D < 250$ Mpc, w : γ-ray 50 GeV-2 TeV.

ω = UHECR flux proxy

Advantages of the present analysis

- Ansatzes for the relative UHECRS fluxes → potentially more sensitive than previous analysis based solely on the source direction
- Improved knowledge of energy-dependent compositions → attenuation fluxes
- Significant increase of the Pierre Auger Observatory exposure → data can reveal more subtle patterns

Search for Intermediate-scale Anisotropies

Analysis strategy

- Sky model probability maps:

Φ_i = flux model x attenuat. model x ang. smearing (σ) x exposure

- Single population signal model H_1:

$$\Phi = (1- f)\, \Phi_0 + f\, \Phi_{i.} \quad \textbf{: (free parameters: } \sigma \textbf{ and f)}$$

- Null hypothesis H_0: isotropy Φ_0
- Test statistics: $TS = 2 \log(H_1/H_0)$
- p-value from Wilk's theorem: $p(TS) = p_{\chi 2}(TS,ndf)$

Test Statistic vs. Energy

SBG fits data better than isotropy at 4σ C.L. (penalized by the energy scan)

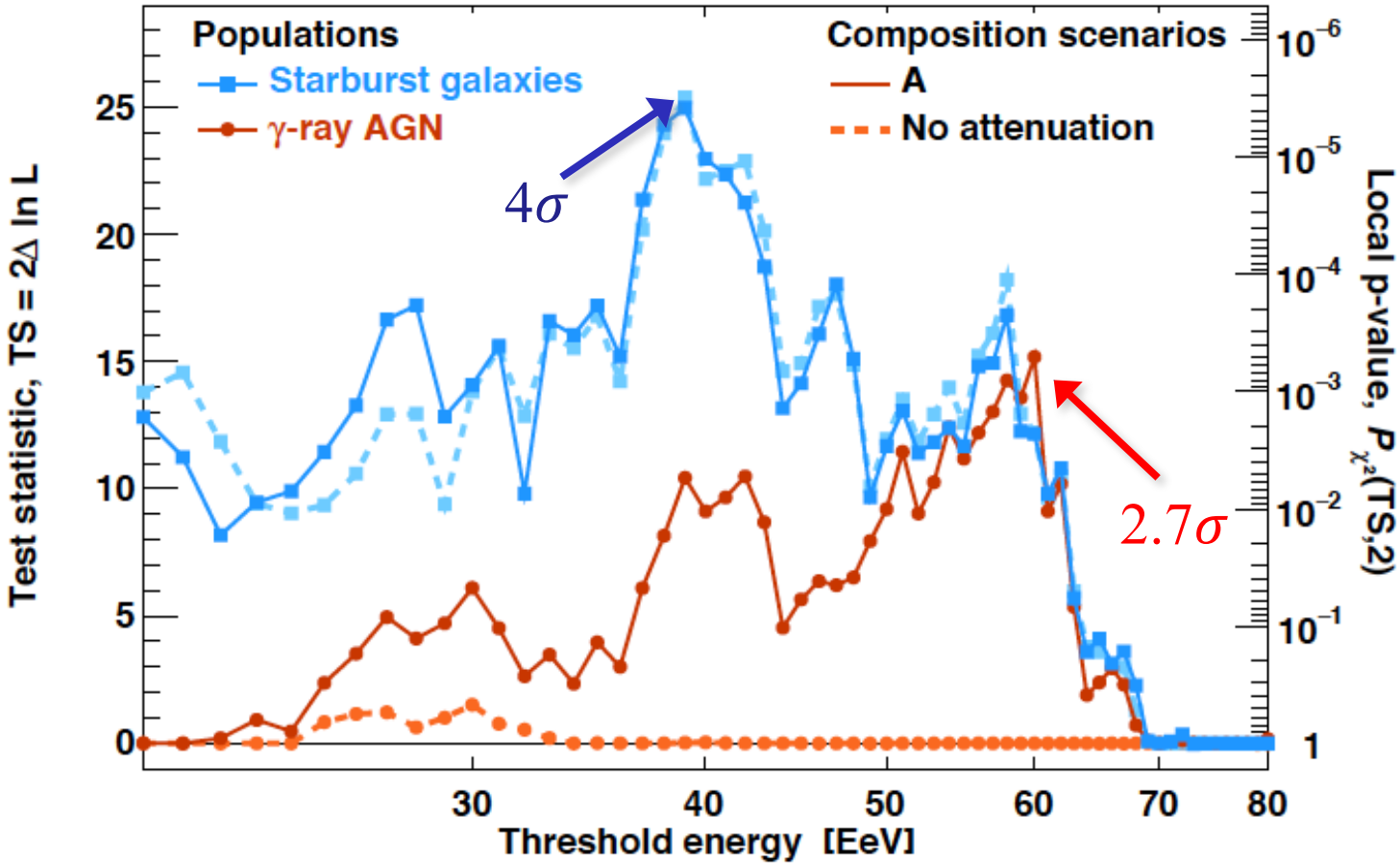

A: Auger best fit ==>

name	lg(R_{max}/V)	f_p	f_{He}	f_N	f_{Si}	γ
EPO1st	18.68	0.000	0.673	0.281	0.046	0.96

Pierre Auger Coll., JCAP **1704** (2017) 038

Best fit parameters

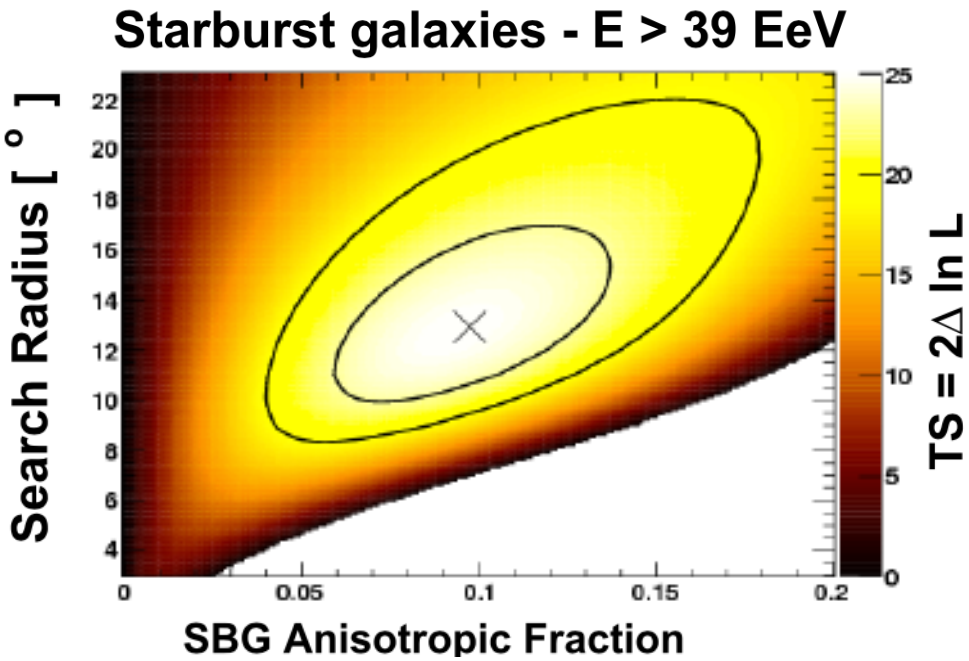

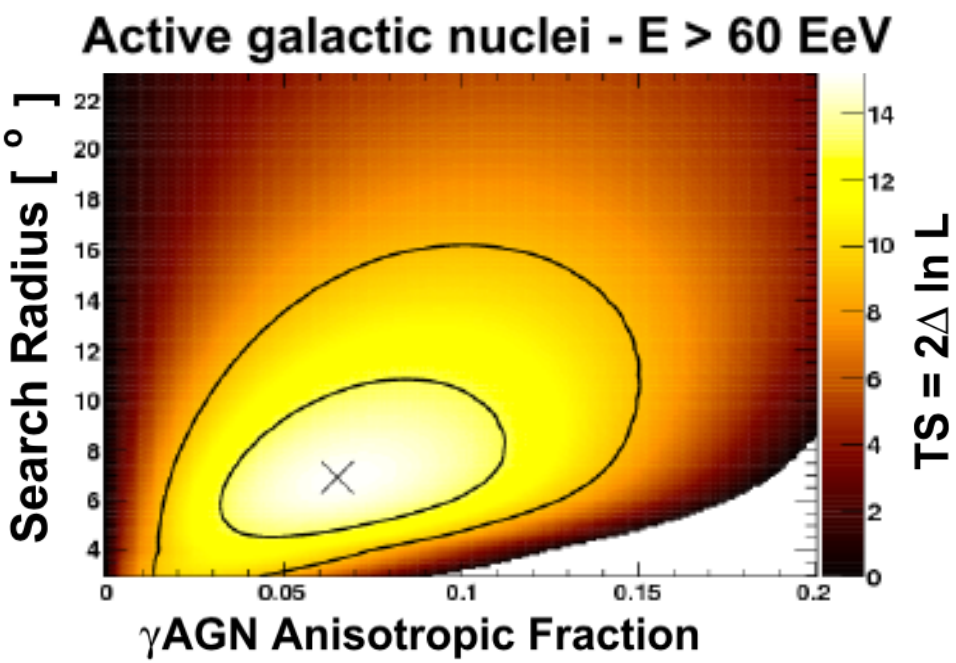

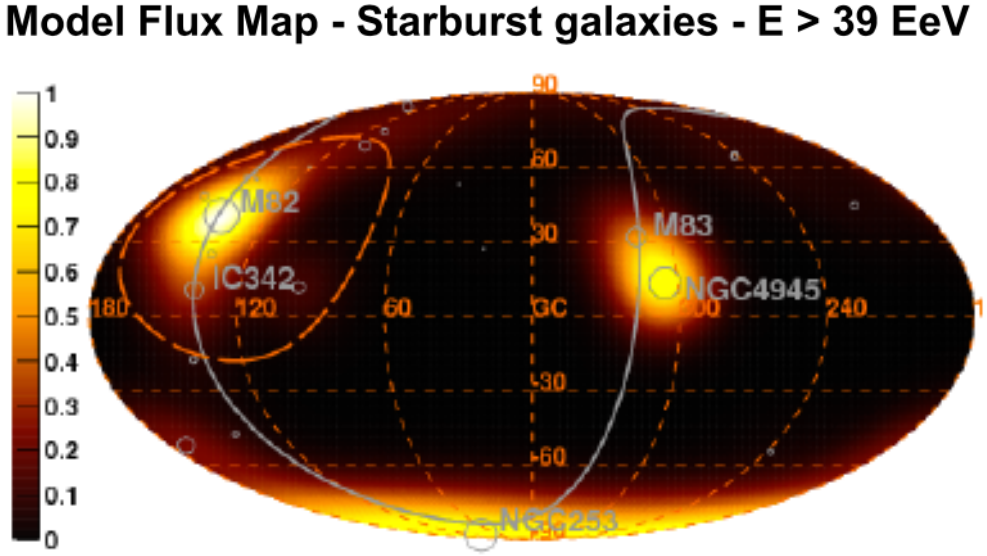

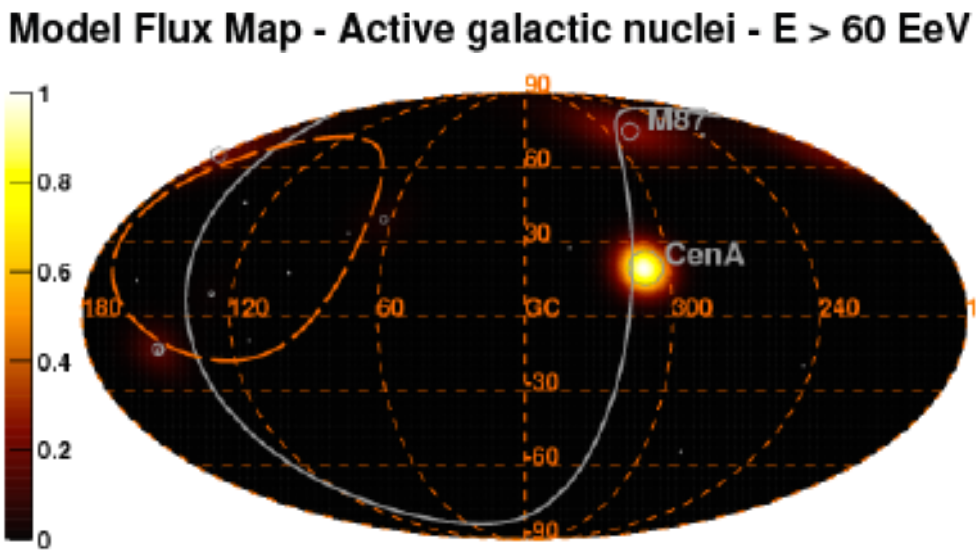

Data vs Model (gal. coordinates)

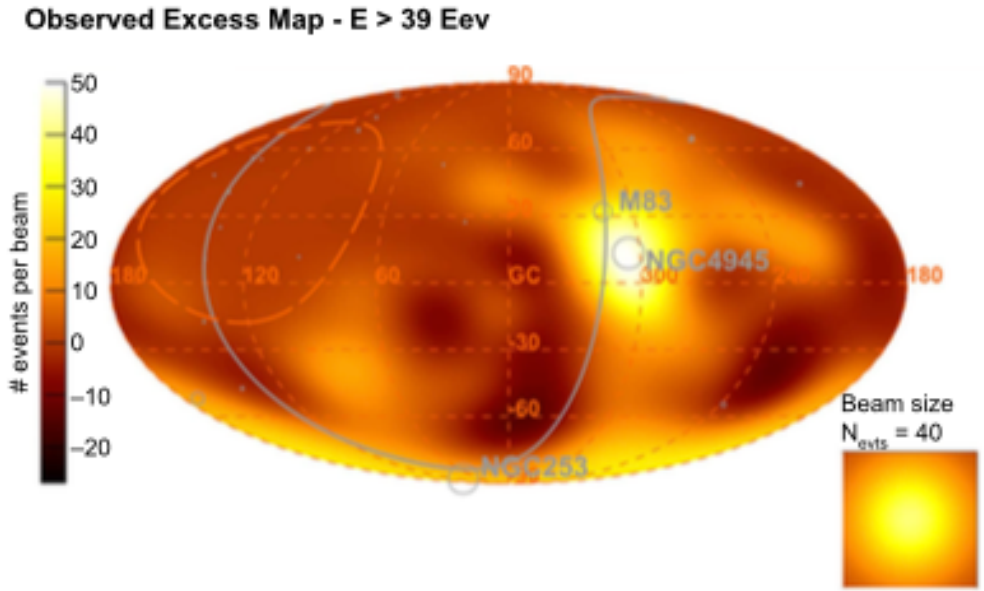

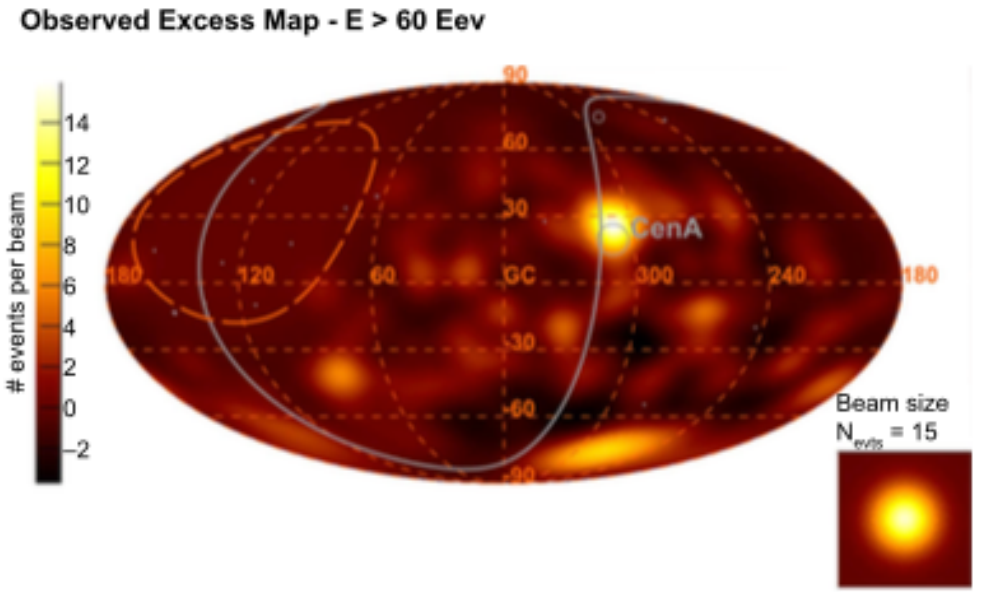

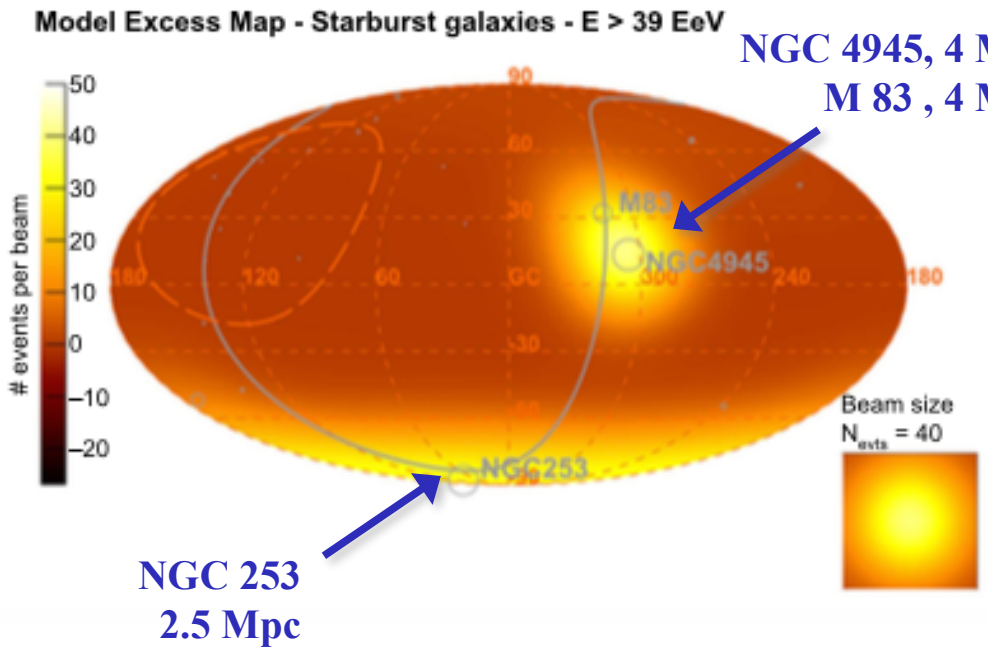

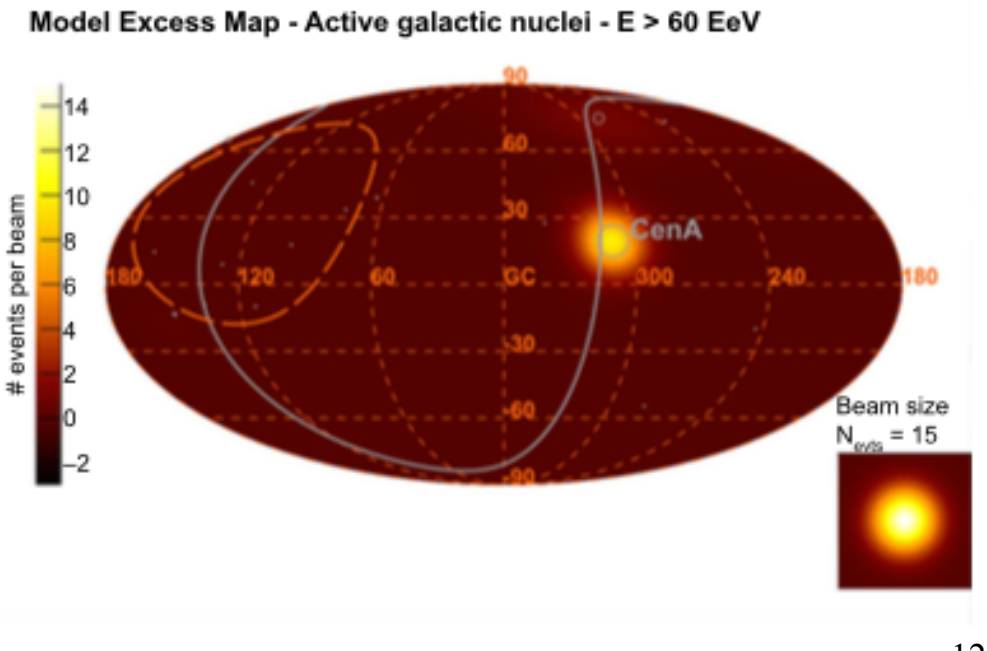

Summary about searches for intermediate-scale anisotropies

- Isotropy of UHECRs is disfavored with 4.0 σ confidence in comparison with SBG model
- Caution is required in identifying SBGs as the preferred sources prior to understanding the impact of the magnetic deflections
- No penalization for multiple searches performed within the Collaboration

Arrival Directions

- Indication for intermediate-scale anisotropy

  ApJ.Lett. 853:L29 (2018)853:L29

- Observation of Large-scale anisotropy

  Science 357 (2017) 1266

  submitted to ApJ, arXiv:1808.03579

Observation of Dipolar anisotropy above 8 EeV

Harmonic analysis in right ascension α

E [EeV]	events	amplitude r	phase [deg.]	$P(\geq r)$
4-8	81701	$0.005^{+0.006}_{-0.002}$	80 ± 60	0.60
> 8	32187	$0.047^{+0.008}_{-0.007}$	100 ± 10	2.6×10^{-8}

significant modulation at 5.2σ (5.6σ before penalization for energy bins explored)

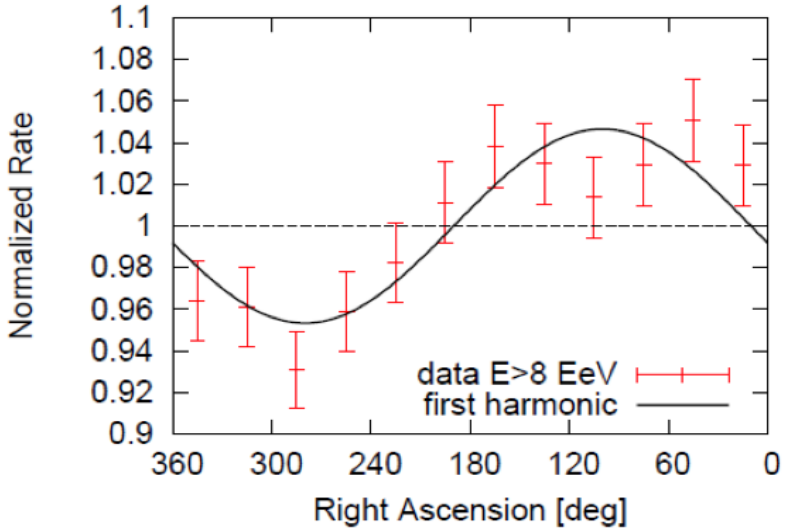

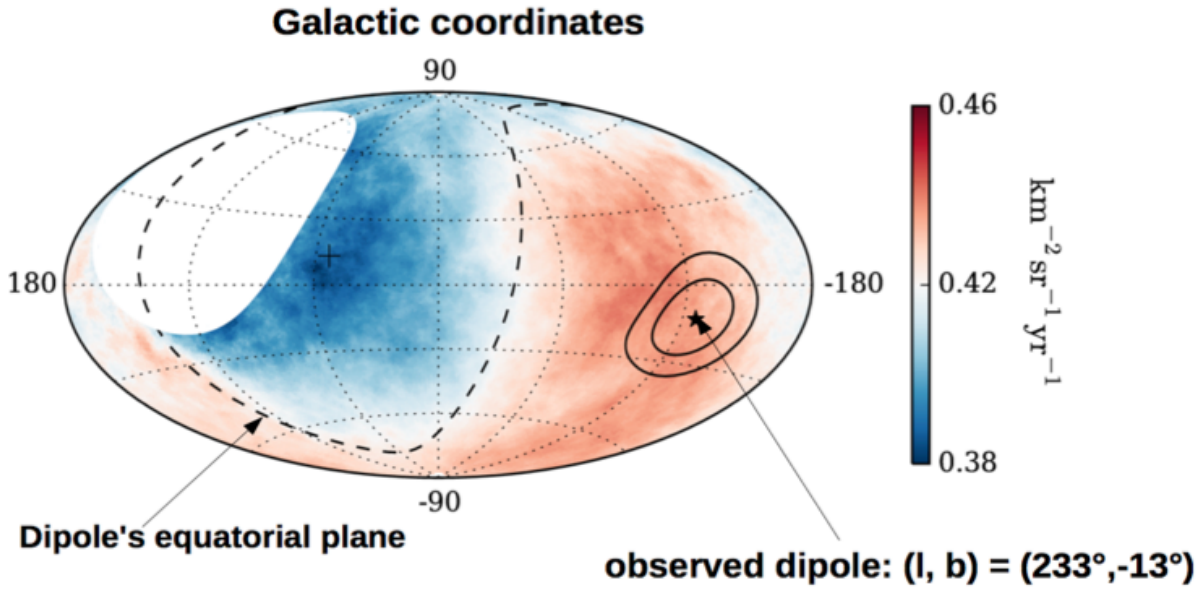

3d-dipole above 8 EeV: $(6.5^{+1.3}_{-0.9})\%$ at $(\alpha, \delta) = (100°, -24°)$

Search for quadrupolar patterns

Table 1. Results of the first and second harmonic analyses in right ascension.

Energy [EeV]	events	k	a_k^α	b_k^α	r_k^α	$\varphi_k^\alpha[^\circ]$	$P(\geq r_k^\alpha)$
4 - 8	81,701	1	0.001 ± 0.005	0.005 ± 0.005	0.005	80 ± 60	0.60
		2	-0.001 ± 0.005	0.001 ± 0.005	0.002	70 ± 80	0.94
≥ 8	32,187	1	-0.008 ± 0.008	0.046 ± 0.008	0.047	100 ± 10	2.6×10^{-8}
		2	0.013 ± 0.008	0.012 ± 0.008	0.018	21 ± 12	0.065

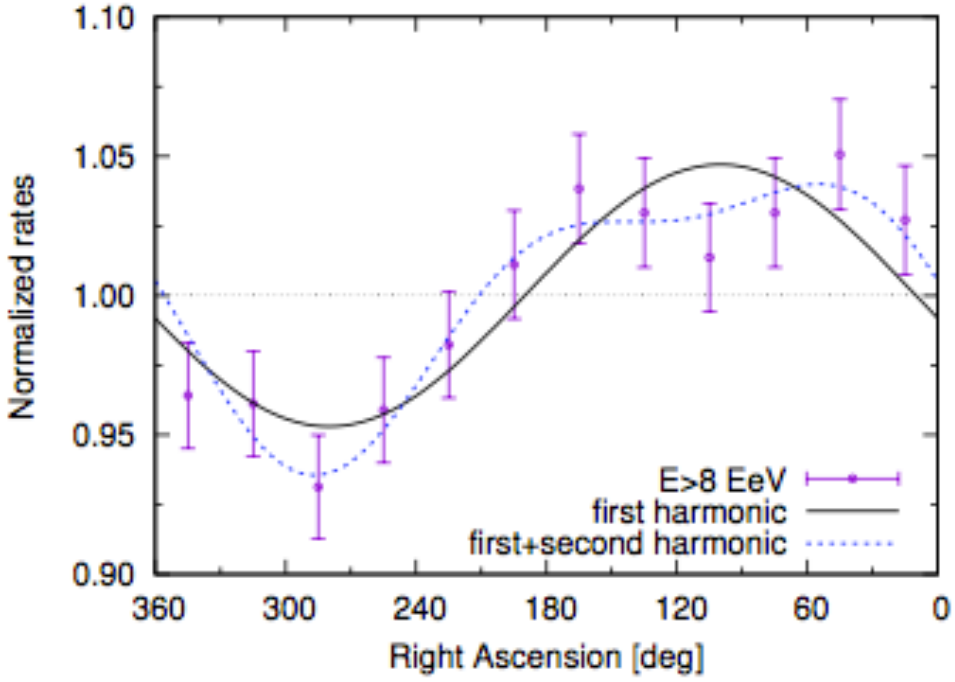

No significant second harmonic amplitude

Energy dependence of dipole amplitude and direction

- Energy bin above 8 EeV splitted in 3: [8,16] EeV, [16,32] EeV and E > 32 EeV

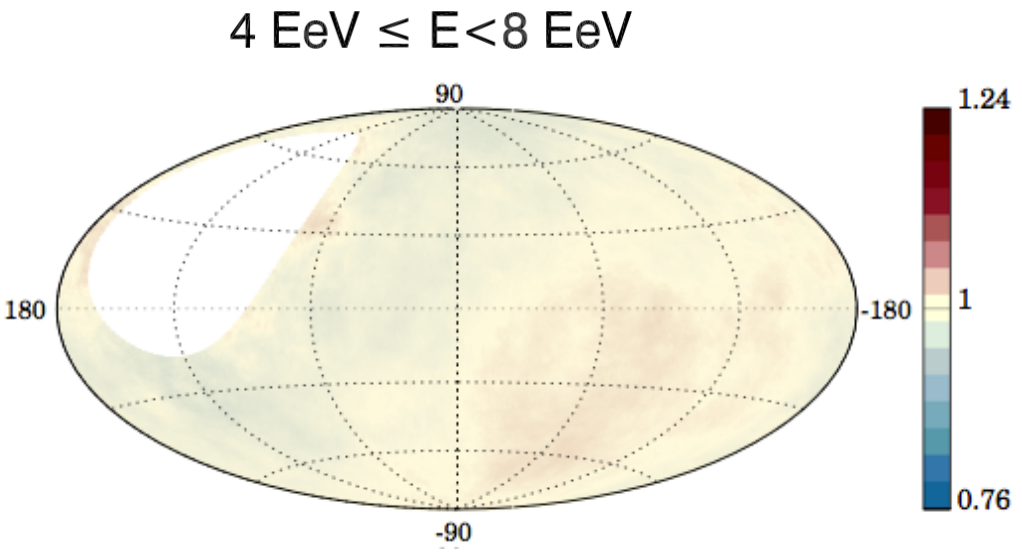

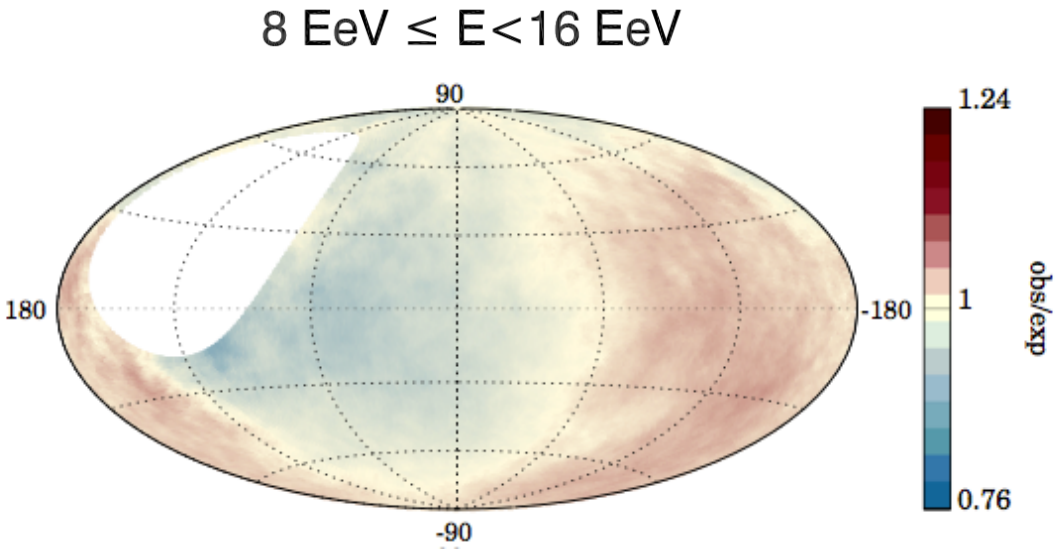

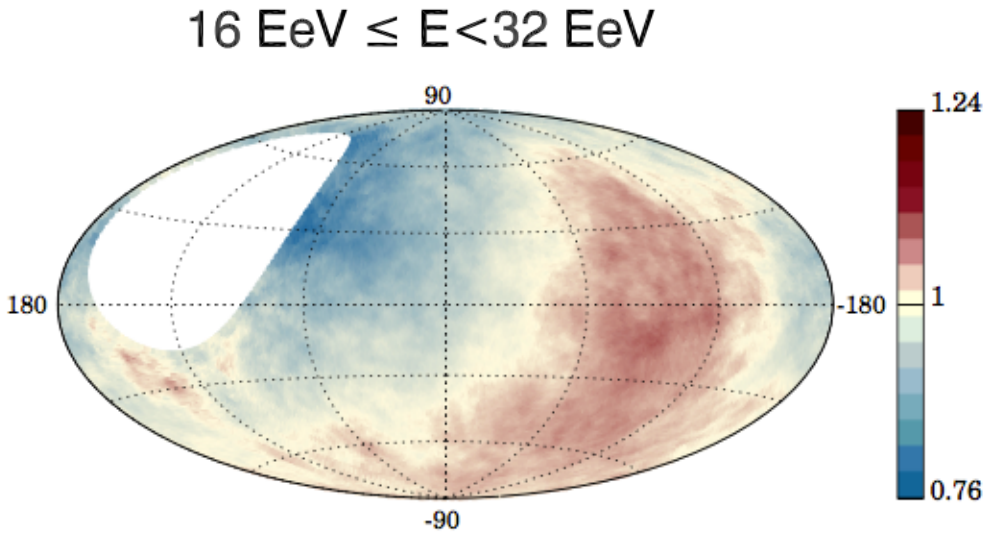

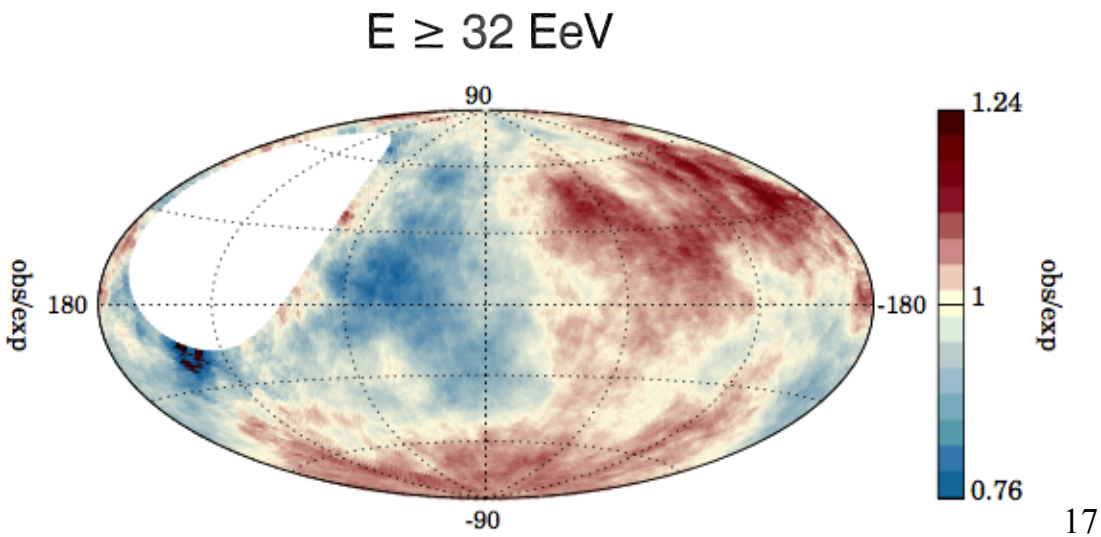

Energy dependence of dipole amplitude and direction

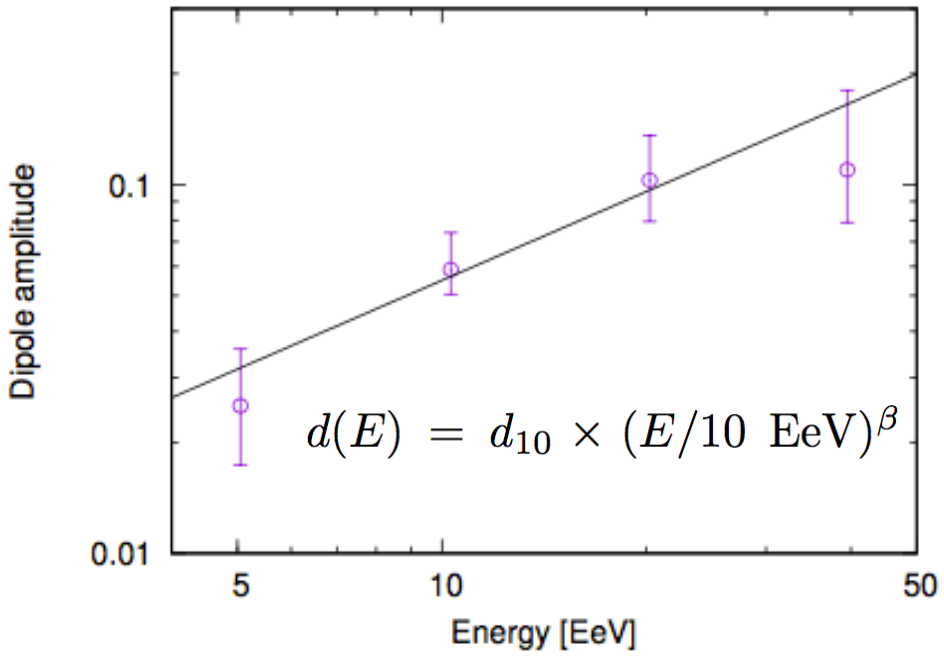

Expected because of the smaller CR deflection at higher rigidities and large attenuation suffered by CRs from distant sources

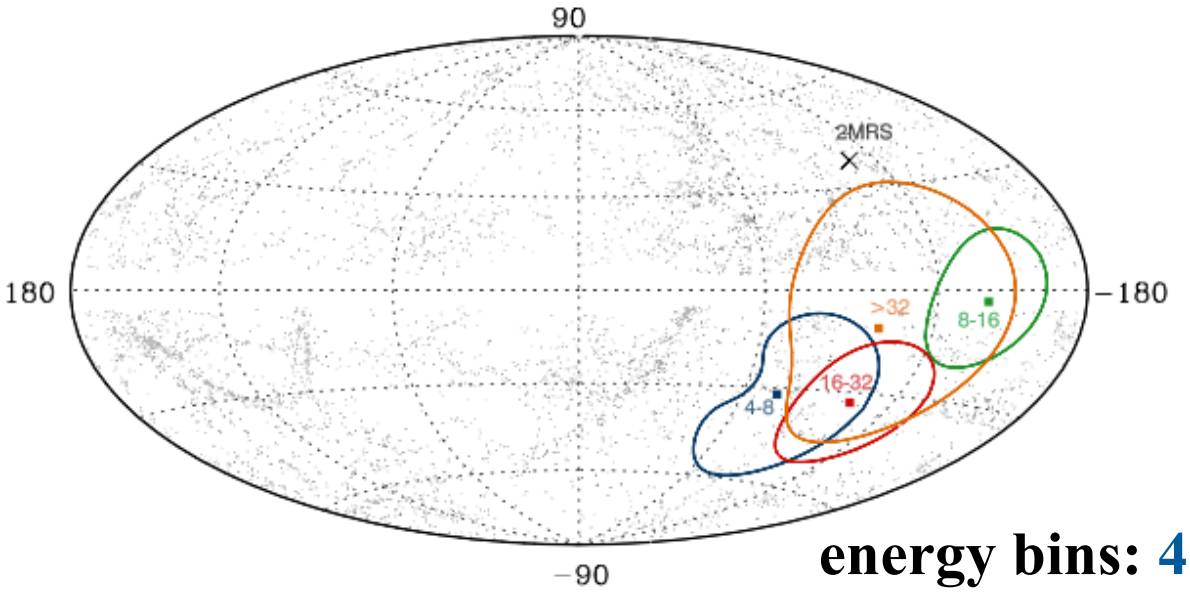

No clear trend in change of dipole direction as a function of energy

energy bins: 4-8, 8-16, 16-32, > 32

Plausible explanations for the dipolar-like structure

Dipole anisotropy may

- arise from diffusive propagation from powerful sources in few nearby galaxies
- reflect known anisotropy in distribution of galaxies within few hundred Mpc

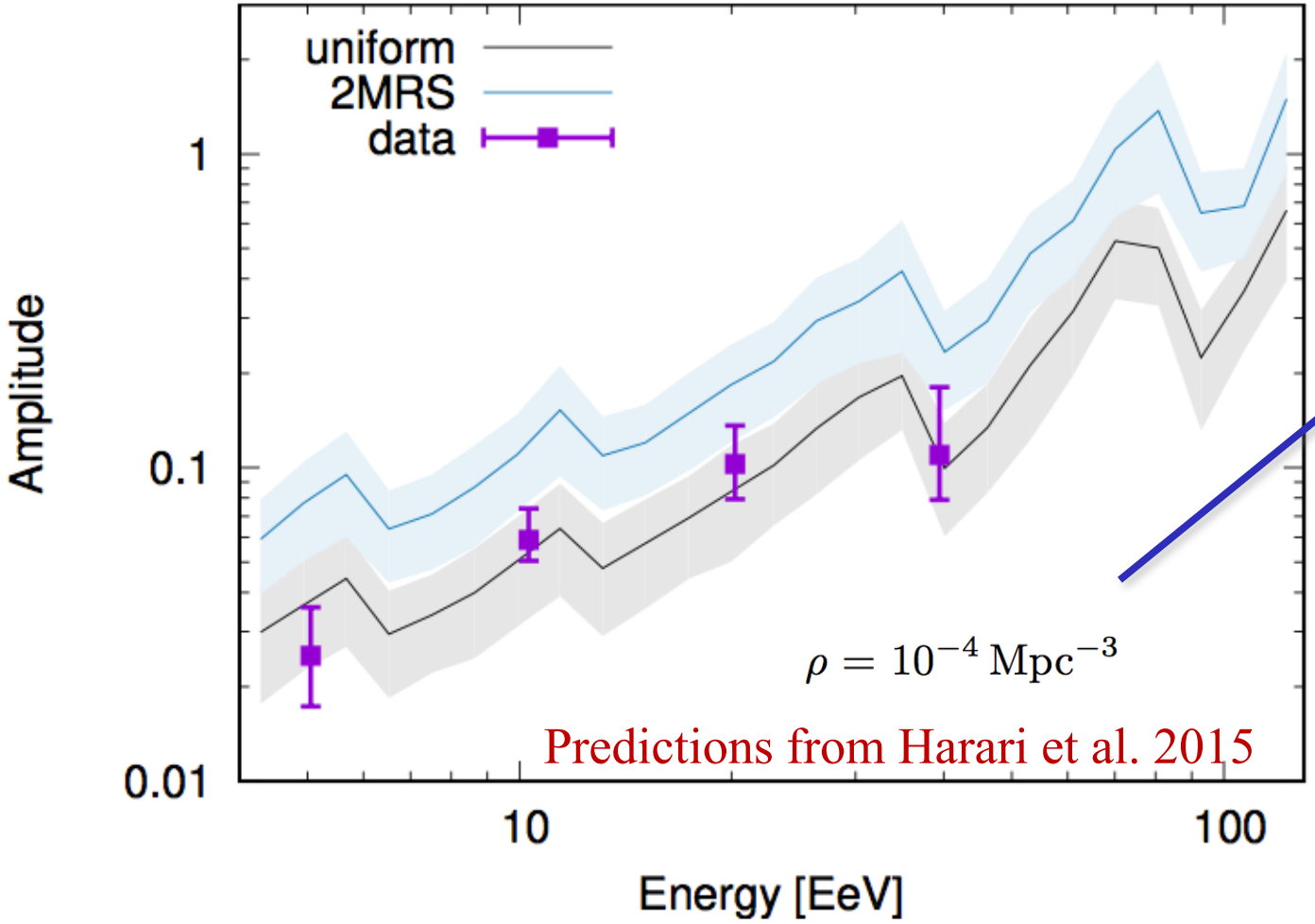

Depends on source density

Conclusions

- **E > 39 EeV:** Indication for intermediate scale anisotropy
- **E> 8 EeV:** Dipolar anisotropy with > 5σ significance
  - dipolar amplitude increases with energy
  - disfavors of galactic origin

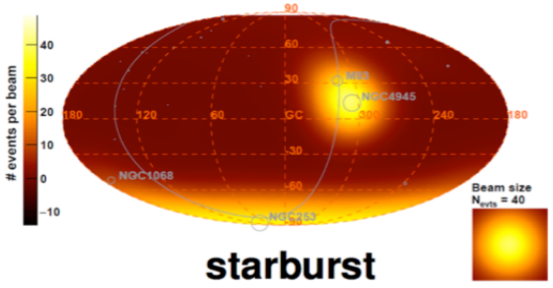

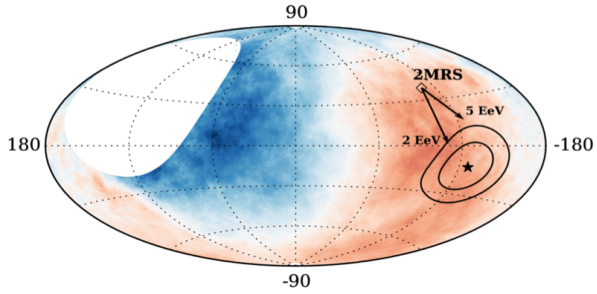

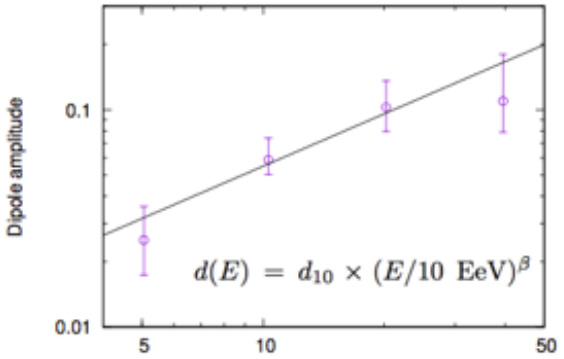

Mass-sensitive observables for each event provided by the upgrade detection of the Pierre Auger observatory will help in the comprehension about the UHECRs

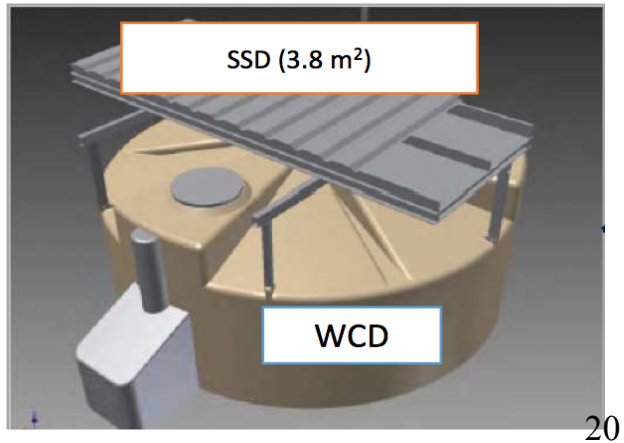

Backups

Populations investigated

SBGs	l (°)	b (°)	Distance[a] (Mpc)	Flux Weight (%)	Attenuated Weight: A/B/C (%)	% Contribution[b]: A/B/C (%)
NGC 253	97.4	−88	2.7	13.6	20.7/18.0/16.6	35.9/32.2/30.2
M82	141.4	40.6	3.6	18.6	24.0/22.3/21.4	0.2/0.1/0.1
NGC 4945	305.3	13.3	4	16	19.2/18.3/17.9	39.0/38.4/38.3
M83	314.6	32	4	6.3	7.6/7.2/7.1	13.1/12.9/12.9
IC 342	138.2	10.6	4	5.5	6.6/6.3/6.1	0.1/0.0/0.0
NGC 6946	95.7	11.7	5.9	3.4	3.2/3.3/3.5	0.1/0.1/0.1
NGC 2903	208.7	44.5	6.6	1.1	0.9/1.0/1.1	0.6/0.7/0.7
NGC 5055	106	74.3	7.8	0.9	0.7/0.8/0.9	0.2/0.2/0.2
NGC 3628	240.9	64.8	8.1	1.3	1.0/1.1/1.2	0.8/0.9/1.1
NGC 3627	242	64.4	8.1	1.1	0.8/0.9/1.1	0.7/0.8/0.9
NGC 4631	142.8	84.2	8.7	2.9	2.1/2.4/2.7	0.8/0.9/1.1
M51	104.9	68.6	10.3	3.6	2.3/2.8/3.3	0.3/0.4/0.5
NGC 891	140.4	−17.4	11	1.7	1.1/1.3/1.5	0.2/0.3/0.3
NGC 3556	148.3	56.3	11.4	0.7	0.4/0.6/0.6	0.0/0.0/0.0
NGC 660	141.6	−47.4	15	0.9	0.5/0.6/0.8	0.4/0.5/0.6
NGC 2146	135.7	24.9	16.3	2.6	1.3/1.7/2.0	0.0/0.0/0.0
NGC 3079	157.8	48.4	17.4	2.1	1.0/1.4/1.5	0.1/0.1/0.1
NGC 1068	172.1	−51.9	17.9	12.1	5.6/7.9/9.0	6.4/9.4/10.9
NGC 1365	238	−54.6	22.3	1.3	0.5/0.8/0.8	0.9/1.5/1.6
Arp 299	141.9	55.4	46	1.6	0.4/0.7/0.6	0.0/0.0/0.0
Arp 220	36.6	53	80	0.8	0.1/0.3/0.2	0.0/0.2/0.1
NGC 6240	20.7	27.3	105	1	0.1/0.3/0.1	0.1/0.3/0.1
Mkn 231	121.6	60.2	183	0.8	0.0/0.1/0.0	0.0/0.0/0.0

Populations investigated

γAGNs	l (°)	b (°)	Distance[a] (Mpc)	Flux Weight (%)	Attenuated Weight: A/B/C (%)	% Contribution[b]: A/B/C (%)
Cen A Core	309.6	19.4	3.7	0.8	60.5/14.6/40.4	86.8/56.3/71.5
M87	283.7	74.5	18.5	1	15.3/7.1/29.5	9.7/12.1/23.1
NGC 1275	150.6	−13.3	76	2.2	6.6/6.1/7.5	0.7/1.6/1.0
IC 310	150.2	−13.7	83	1	2.3/2.4/2.6	0.3/0.6/0.3
3C 264	235.8	73	95	0.5	0.8/1.0/0.8	0.4/1.3/0.5
TXS 0149 + 710	127.9	9	96	0.5	0.7/0.9/0.7	0.0/0.0/0.0
Mkn 421	179.8	65	136	54	11.4/48.3/14.7	1.8/19.1/2.8
PKS 0229-581	280.2	−54.6	140	0.5	0.1/0.5/0.1	0.2/2.0/0.3
Mkn 501	63.6	38.9	148	20.8	2.3/15.0/3.6	0.3/5.2/0.6
1ES 2344 + 514	112.9	−9.9	195	3.3	0.0/1.0/0.1	0.0/0.0/0.0
Mkn 180	131.9	45.6	199	1.9	0.0/0.5/0.0	0.0/0.0/0.0
1ES 1959 + 650	98	17.7	209	6.8	0.0/1.7/0.1	0.0/0.0/0.0
AP Librae	340.7	27.6	213	1.7	0.0/0.4/0.0	0.0/1.3/0.0
TXS 0210 + 515	135.8	−9	218	0.9	0.0/0.2/0.0	0.0/0.0/0.0
GB6 J0601 + 5315	160	14.6	232	0.4	0.0/0.1/0.0	0.0/0.0/0.0
PKS 0625-35	243.4	−20	245	1.3	0.0/0.1/0.0	0.0/0.5/0.0
I Zw 187	77.1	33.5	247	2.3	0.0/0.2/0.0	0.0/0.0/0.0

Combined Fit (Xmax and spectrum) of Auger data

Identical sources homogeneously distributed in a comoving volume

• Injection consisting only of H, He, Ni, Si and Fe (approximately equally space in ln A)

• Power low spectrum with rigidity-dependent exponentital cuttof

$$\frac{dN_{inj,i}}{dE} = \begin{cases} J_0 p_i \left(\frac{E}{E_0}\right)^{-\gamma}, & E/Z_i < R_{cut} \\ J_0 p_i \left(\frac{E}{E_0}\right)^{-\gamma} \exp\left(1 - \frac{E}{Z_i R_{cut}}\right), & E/Z_i > R_{cut\,He}, \end{cases}$$

p_{Ni} and p_{Si})

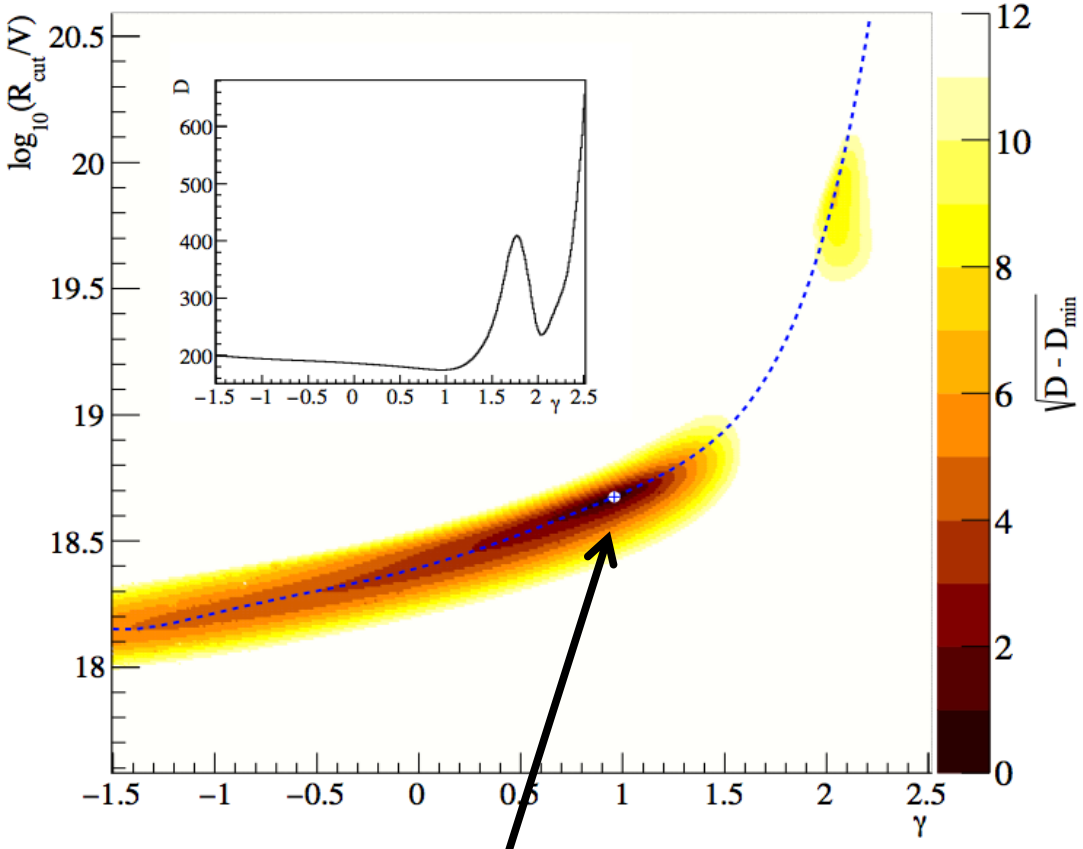

Best Fit

• Hard spectral index
• Low Cutoff energy
Exhaustion of source scenario favored

Caveat: dependence of the propagation models

Combined Fit (Xmax and spectrum) of Auger data

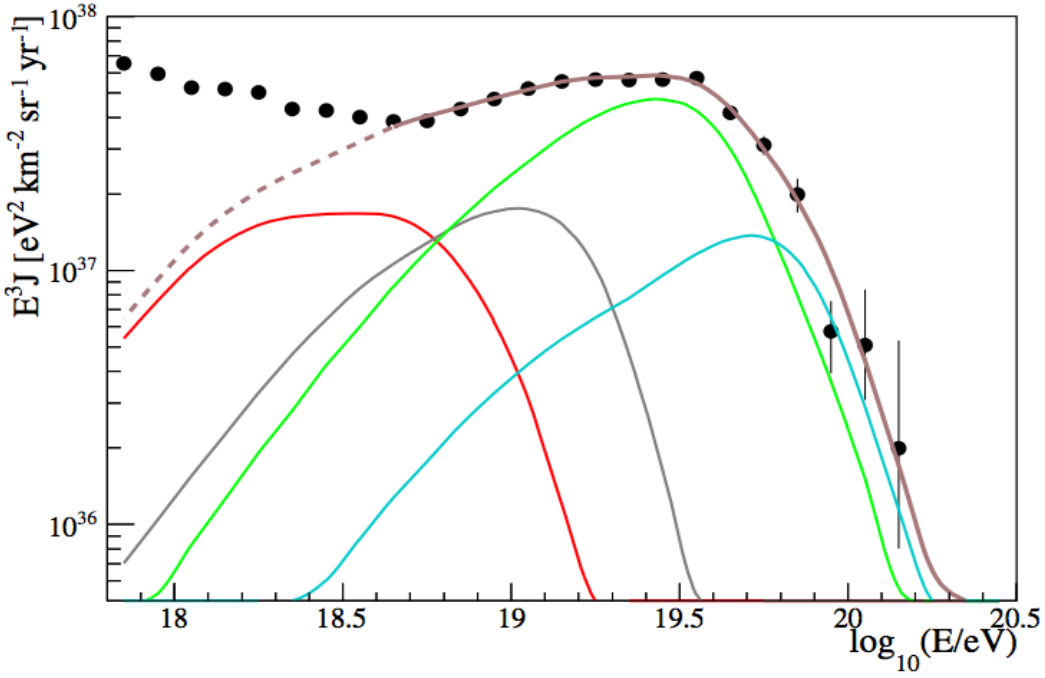

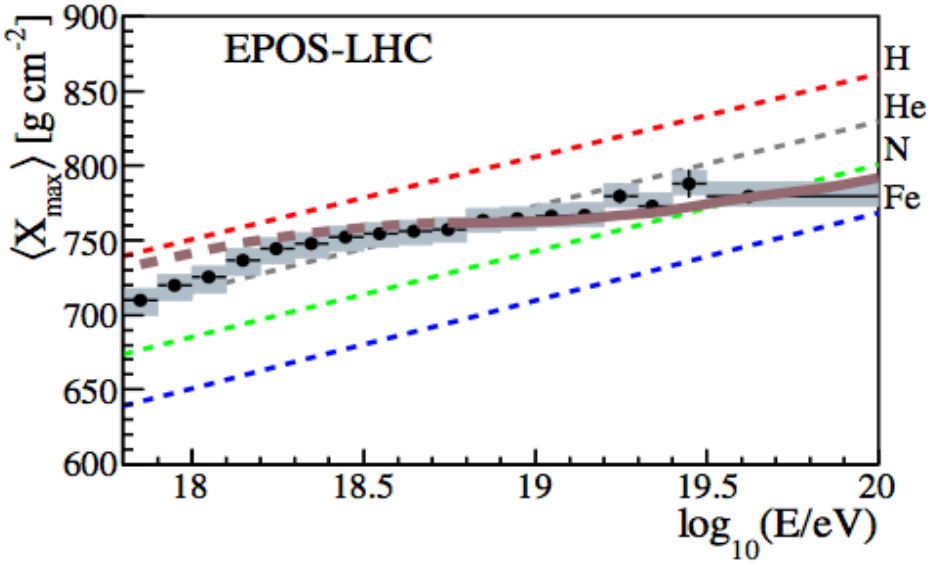

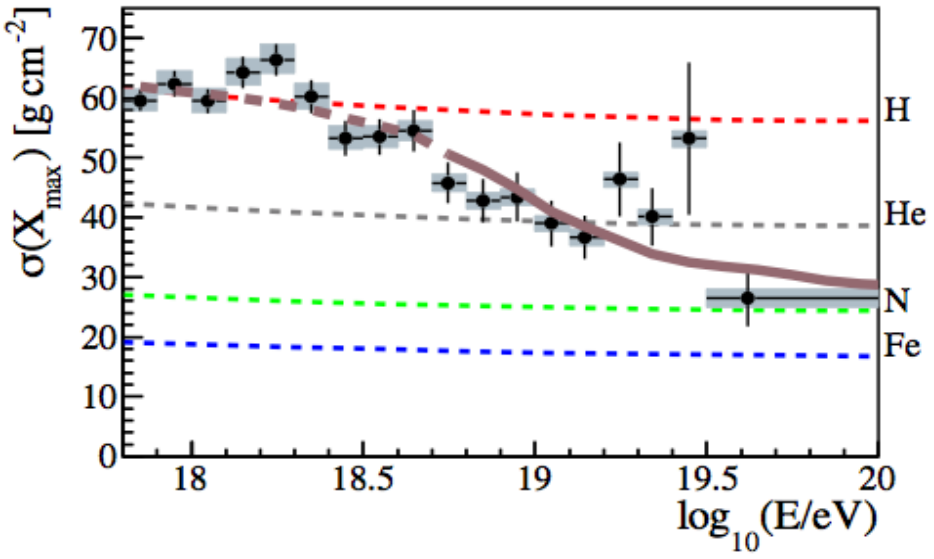

Tests with different hypotheses

Test hypothesis	Null hypothesis	Threshold energy[a]	TS	Local p-value $\mathcal{P}_{\chi^2}(\mathrm{TS}, 2)$	Post-trial p-value	1-sided significance	AGN/other fraction	SBG fraction	Search radius
SBG + ISO	ISO	39 EeV	24.9	3.8×10^{-6}	3.6×10^{-5}	$4.0\,\sigma$	N/A	9.7 %	12.9°
γAGN + SBG + ISO	γAGN + ISO	39 EeV	14.7	N/A	1.3×10^{-4}	$3.7\,\sigma$	0.7 %	8.7 %	12.5°
γAGN + ISO	ISO	60 EeV	15.2	5.1×10^{-4}	3.1×10^{-3}	$2.7\,\sigma$	6.7 %	N/A	6.9°
γAGN + SBG + ISO	SBG + ISO	60 EeV	3.0	N/A	0.08	$1.4\,\sigma$	6.8 %	0.0 %[b]	7.0°
Swift-BAT + ISO	ISO	39 EeV	18.2	1.1×10^{-4}	8.0×10^{-4}	$3.2\,\sigma$	6.9 %	N/A	12.3°
Swift-BAT + SBG + ISO	*Swift*-BAT + ISO	39 EeV	7.8	N/A	5.1×10^{-3}	$2.6\,\sigma$	2.8 %	7.1 %	12.6°
2MRS + ISO	ISO	38 EeV	15.1	5.2×10^{-4}	3.3×10^{-3}	$2.7\,\sigma$	15.8 %	N/A	13.2°
2MRS + SBG + ISO	2MRS + ISO	39 EeV	10.4	N/A	1.3×10^{-3}	$3.0\,\sigma$	1.1 %	8.9 %	12.6°

[a] For composite model studies, no scan over the threshold energy is performed.

[b] Maximum TS reached at the boundary of the parameter space.

ISO: isotropic model.

Optimization: signal fraction and angular smearing

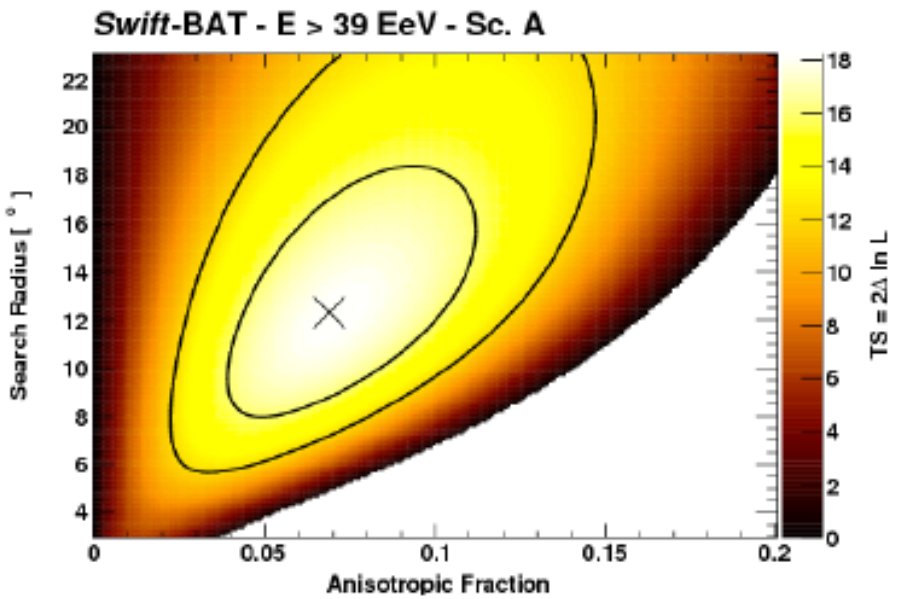

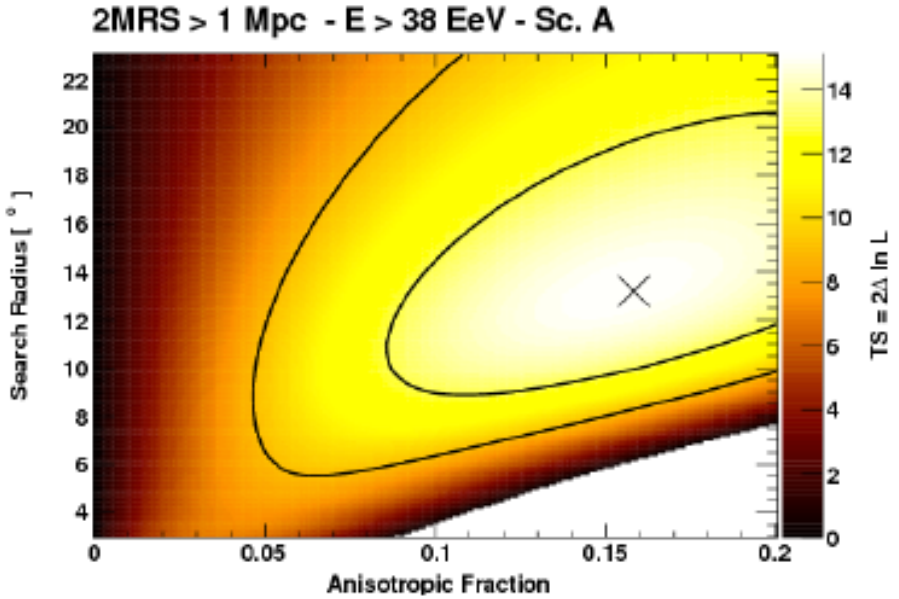

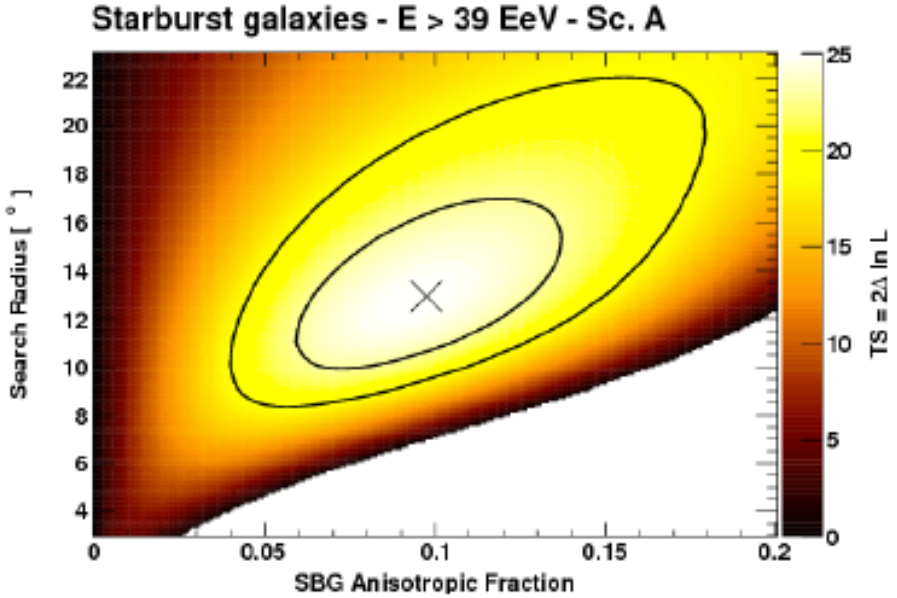

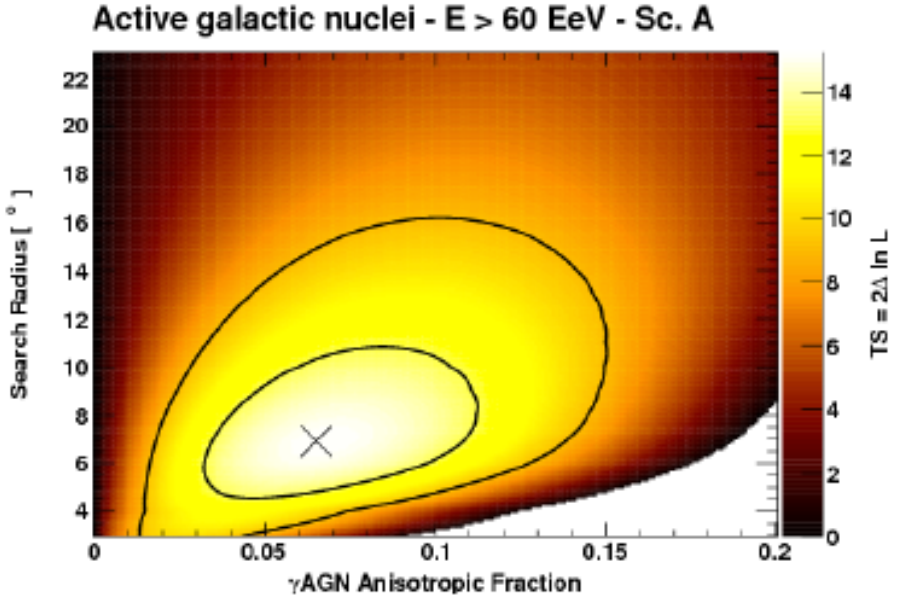

Galactic origin?

- MC: estimate flux at the Earth from a continuous distribution of sources with a density proportional to that of the luminous matter taking into account magnetic deflections

  ==> Dipole directions close to Galactic center

  ==> Dipole amplitudes too large for Galactic cosmic-ray origins (> 0.8)

  Unlikely of galactic origin!!

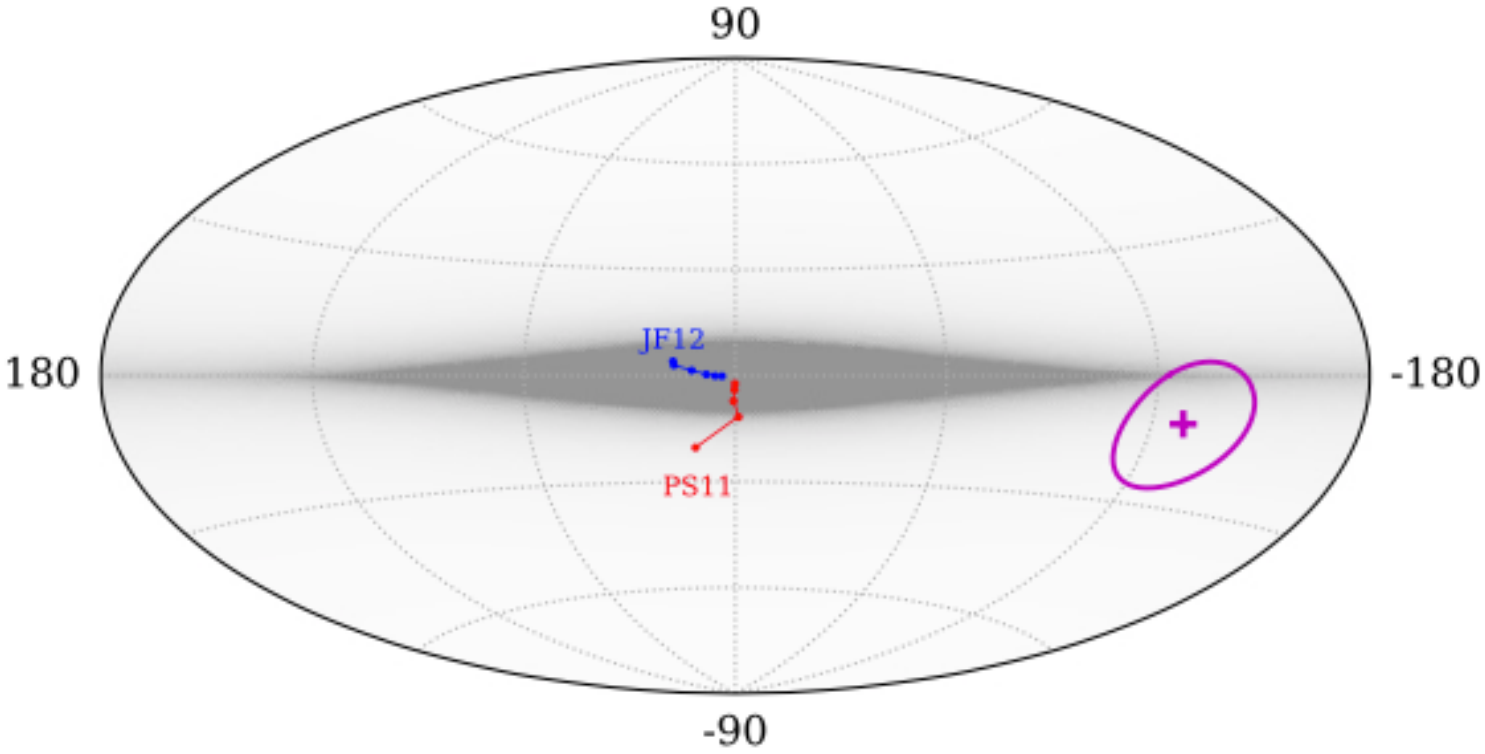

Change of X-Gal dipole direction after Gal. Magnetic Field (JF12)

- Arrows start at extragalactic directions → reconstruct on Earth for different CR rigidities
- Extragalactic dipoles at positive galactic longitudes align close to inner spiral arm, opposite half to outer spiral arm

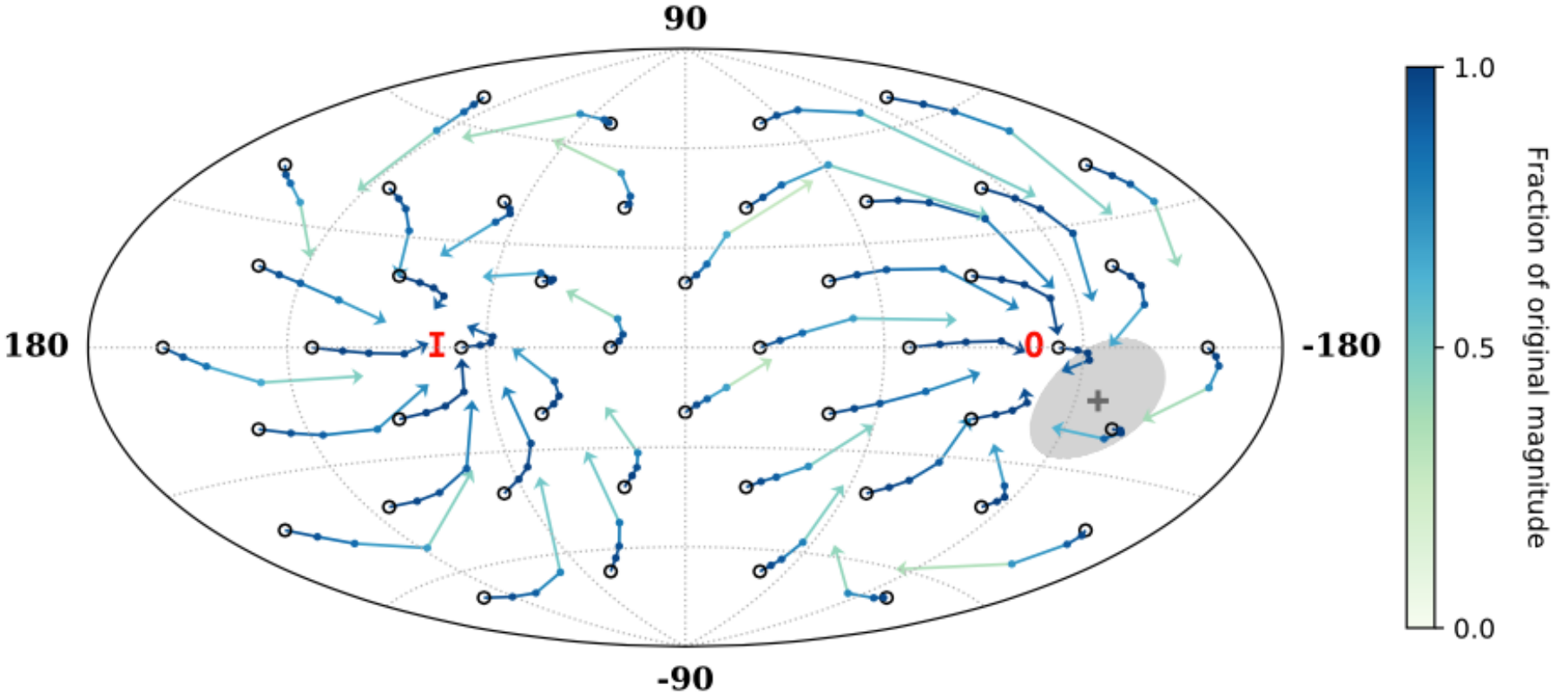

Change of X-Gal dipole direction after Gal. Magnetic Field (JF12)

- Arrows start at extragalactic directions → reconstruct on Earth for different CR rigidities
- Extragalactic dipoles at positive galactic longitudes align close to inner spiral arm, opposite half to outer spiral arm

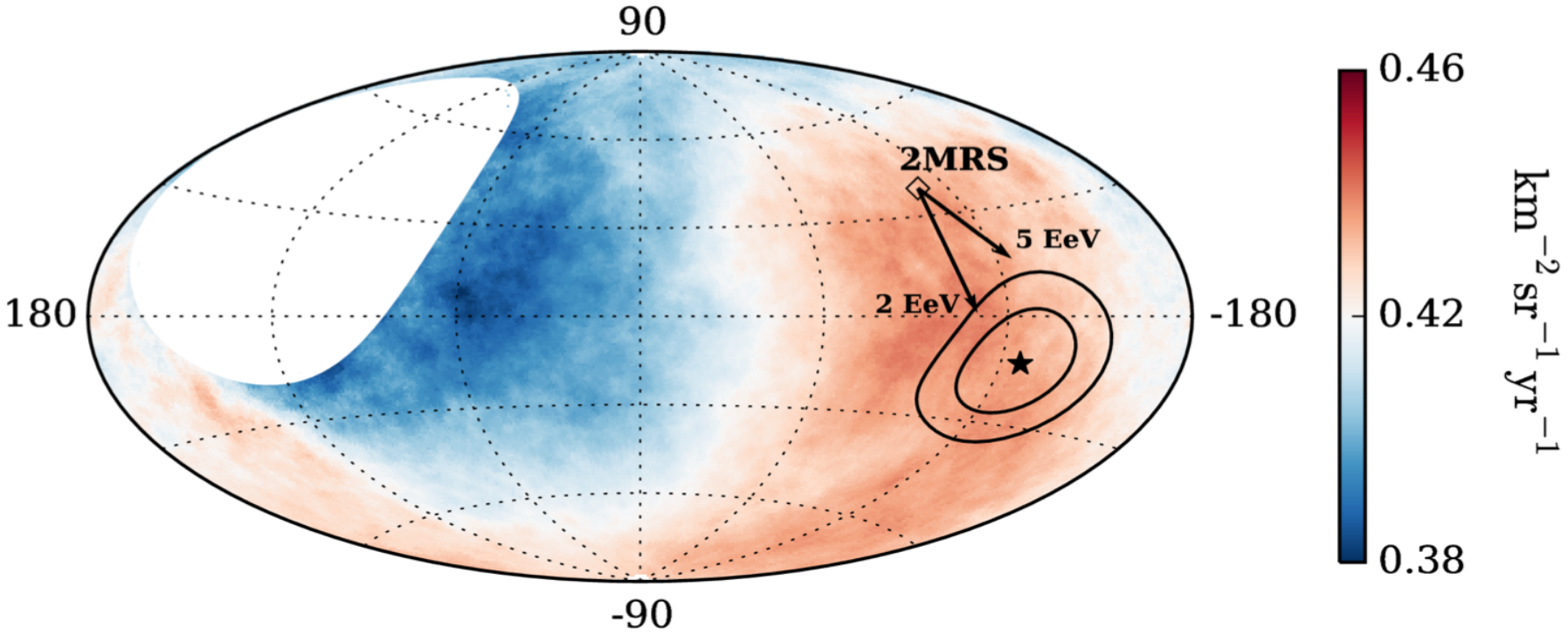

Dipole above 8 EeV in Eq. coordinates

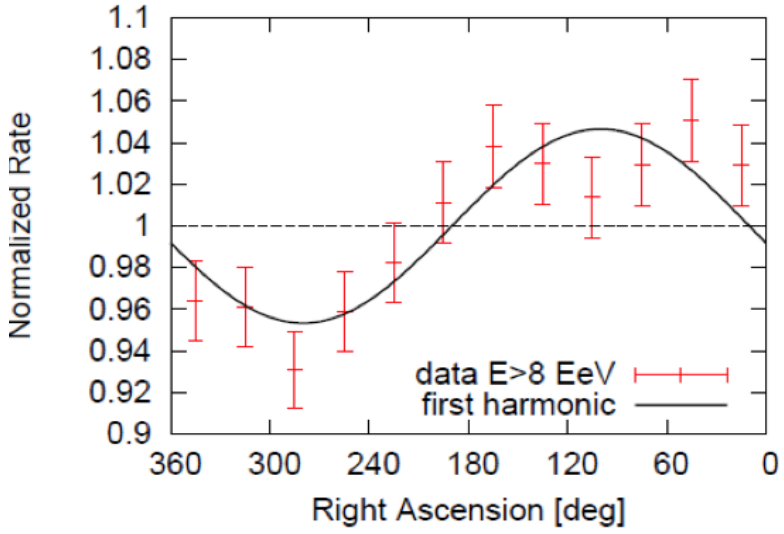

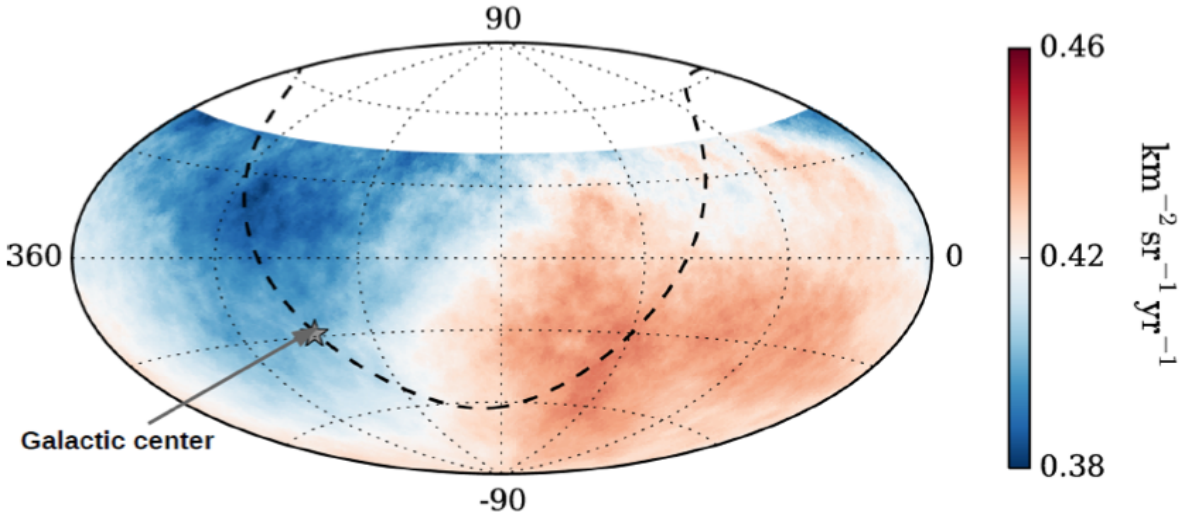

3D dipole → $(6.5^{+1.3}_{-0.9})\%$ at $(\alpha, \delta) = (100°, -24°)$

dipole direction ~ 125° from GC ⟹ **disfavors galactic origin**

Model:

Φ_i = flux model x attenuat. model x ang. smearing (σ) x exposure

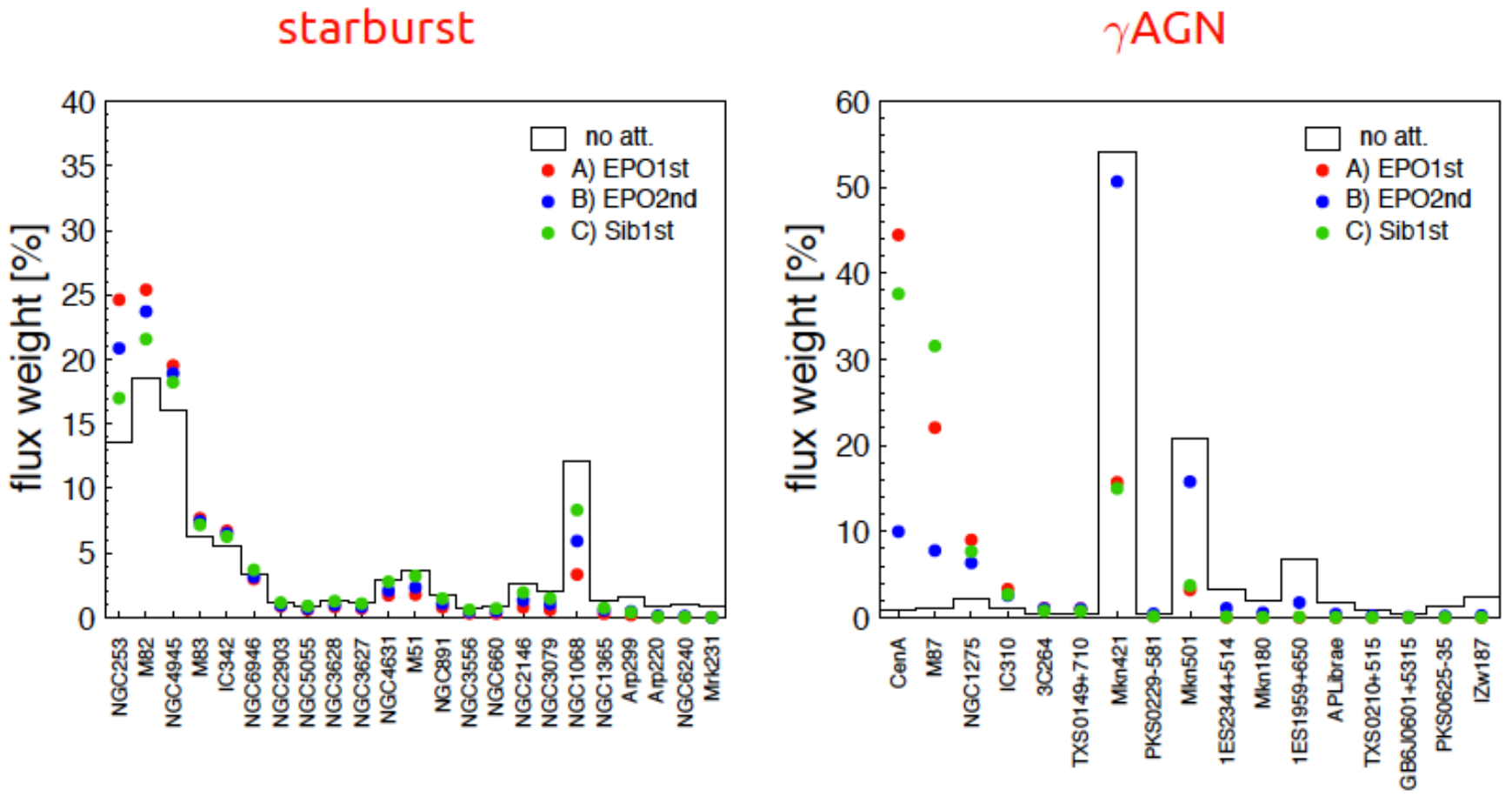

composition scenarios from Pierre Auger Coll., JCAP **1704** (2017) 038 + CRPropa3

name	$\lg(R_{max}/V)$	f_p	f_{He}	f_N	f_{Si}	γ
EPO1st	18.68	0.000	0.673	0.281	0.046	0.96
EPO2nd	19.88	0.000	0.000	0.798	0.202	2.04
Sib1st	18.28	0.702	0.295	0.003	0.000	-1.50

Test Statistic vs. Energy

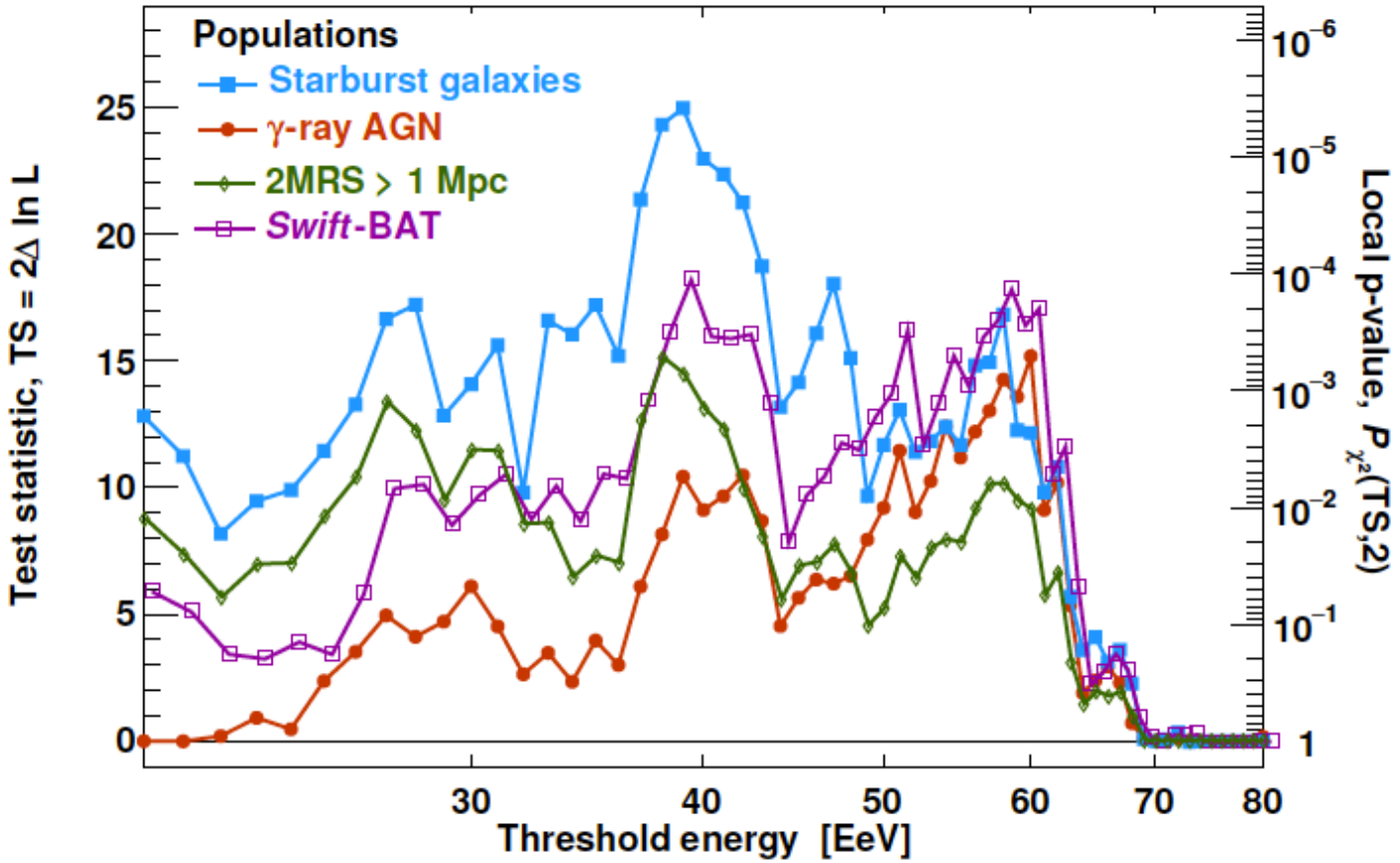

- Caution is required in identifying SBGs as the preferred sources prior to understanding the impact of the magnetic deflections
- No penalization for multiple searches conducted within the Collaboration